Communications System Performance and Design in the Presence of Radar Interference

Narueporn Nartasilpa, Ahmad Salim, Daniela Tuninetti, and Natasha Devroye

***Abstract*— Increasing demands for spectrum have necessitated the coexistence of communications and radar systems within the same band. This paper investigates how an unaltered radar system affects the performance of a communications receiver. For a single-carrier communications system, it is shown that a low power radar signal can be treated as Gaussian noise while a strong radar signal can be subtracted off the received signal, but in doing so one of the two signal dimensions is lost. Complex-valued constellation design problems are next proposed, with the goal of either minimizing the error rate under a power constraint, or maximizing the transmission rate under both error rate and power constraints. Numerically, the designed constellation is shaped as a concentric hexagon for weak radar interference while it morphs into an uneven pulse amplitude modulation for strong interference. A multi-carrier orthogonal frequency division multiplexing communications system is lastly considered. Due to the radar interference, the received signal becomes correlated over time and across carriers. To reduce the complexity of the optimal receiver, several suboptimal decoders are analyzed, among which the one that discards the correlations between subcarriers is numerically found to perform close to the optimal one.**

***Index Terms*— Spectrum sharing, radar interference, communications system, OFDM.**

I. Introduction

ONE solution to the problem of ever-increasing demands for spectrum by wireless services is to allow communications systems to utilize spectrum traditionally allocated to radar systems. This has prompted a great deal of research on radar-communications spectrum sharing [1], [2], in particular in the S-band (2-4 GHz), where communications systems (e.g., WiFi and Long-Term Evolution (LTE)) and radar systems (e.g., Air Traffic Control (ATC), Navy surveillance, and weather) operate. When the two systems co-exist in the same band and operate at the same time, they interfere with one another. Novel solutions for efficient and fair spectrum sharing are needed.

One straightforward solution is to split the available resources (in time or frequency) through policy so that each system operates independently and interference is avoided altogether. For example, Shajaiah *et al.* [3] proposed a time-frequency (carrier by carrier) resource allocation algorithm for co-existing LTE advanced cellular and S-band radar systems. Such resource allocation schemes lead to orthogonal resource allocation, quite different from the simultaneous, overlapping frequency spectrum sharing studied here.

Another solution to the spectrum sharing problem is to retrofit one system so as to better withstand the effect of the other when they operate over the same time and frequency bands. For example, how to spectrally shape a radar waveform such that the radar's detection performance is not compromised while ensuring that legacy communications systems keep their error rates close to the interference-free scenario is considered in [4]. The work in [5] proposed adding a column interleaver/de-interleaver and a log likelihood ratio mapping function to a Wi-Fi system to mitigate the impact of the unaltered radar interference. The work discussed here falls into this retro-fitting category, where we look at how the communications system can alter its transmit and receive chains to better withstand the effect of radar interference.

Rather than retrofitting one system, one could opt to re-design and co-design both the communications and radar systems. In [6], it was concluded that a co-design is key in improving the performance of co-existing architectures, and co-designs have attracted much recent attention, see for example [7] and references therein. In contrast to the resource allocation (orthogonalizing) approach of [3], a framework for a joint radar-communications system was introduced in [8], where only one transmitted signal (decoupled into training and data portions) is used for simultaneous operations for both systems. The optimal training signals are shown to produce the largest lower bound on the communications rate as well as the maximum probability of detection. The work in [8] considered a scenario where both the radar and communications systems share a transmitter and receiver. Waveform design is another popular co-design scheme. This technique utilizes the characteristics of the other system's signal so as to improve each system's performance through carefully designing their transmitted waveforms [9]–[12]. These co-design schemes differ from the presented scheme here, in which the radar system is left unaltered.

OFDM-based co-existence has also been of recent interest. For example, a co-operative spectrum sharing scheme for a matrix completion based colocated Multiple Input Multiple Output (MIMO) radar and MIMO communications systems was presented in [13]. There, transmit precoding at the radar and the communications system antennas is used to maximize the radar signal-to-interference-plus-noise-ratio while meeting certain communications rate and power constraints. An LTE

Manuscript received September 7, 2017; revised January 31, 2018; accepted March 29, 2018. Date of publication April 6, 2018; date of current version September 14, 2018. This work was supported by the National Science Foundation, Grant 1443967. The associate editor coordinating the review of this paper and approving it for publication was A. Tajer. *(Corresponding author: Narueporn Nartasilpa.)*

The authors are with the Department of Electrical and Computer Engineering, University of Illinois at Chicago, Chicago, IL 60607 USA (e-mail: nnarta2@uic.edu; ahmads@uic.edu; danielat@uic.edu; devroye@uic.edu).

Color versions of one or more of the figures in this paper are available online at http://ieeexplore.ieee.org.

Digital Object Identifier 10.1109/TCOMM.2018.2823764

packet scheduling algorithm, based on channel sensing, was proposed in [14] for spectrum allocation for an LTE system during the period between radar pulses resulting in a slight performance degradation for the LTE system. Wang *et al.* [15] concluded that moderate frequency and range separation makes the spectrum sharing between a scanning ATC radar and an LTE cellular network possible with tolerable performance degradations.

While there have been many studies on how radar and communications systems can co-exist within tolerable performance degradation, clear insights on how unaltered radar and communications systems affect one another has not been investigated much despite its relevance to better determine which technology should be pursued for reliable radar-communications coexistence. Herein, our research is mainly focused on the performance of a communications receiver with interference from unaltered radar signals. The findings of this work are relevant for systems where changing the hardware may be too costly, but further digital signal processing of the baseband received signal is viable. This work, together with the results on the probabilities of detection and false alarm of a radar system with interfering unaltered communications signals in [16], can be used to benchmark the performance of actual co-design schemes (where both systems are altered).

This paper focuses on two types of communications systems: a single-carrier, and a multi-carrier systems. It is in part based on our prior conference work, where we analyzed the error rate performance [17] and the constellation design [18] for a single-carrier communications system interfered by a radar signal. In this journal paper, we also report on the error rate performance of a multi-carrier communications system. The channel model utilized in both scenarios is taken from [19], where we derived a model for the radar interference at an OFDM receiver. The contributions of this paper are:

1) An in-depth analysis of a single-carrier communications system suffering from weak, intermediate, and strong radar interference including the system model, detection schemes, and error performances.
2) Design of two-dimensional signal constellations in the low and high radar interference regimes, based on two different problems: maximizing the transmission rate subject to average power and error rate constraints, and minimizing the symbol error rate subject to average power and fixed rate constraints.
3) Comprehensive numerical evaluations of the error rate performance for the optimal Maximum Likelihood (ML) and of suboptimal decoders in an OFDM-based multi-carrier communications system with additive white Gaussian noise and rectangular-pulsed radar interference.
4) Identifying as the best performing suboptimal receiver the one that only accounts for time correlation but discards frequency correlation, and whose error rate performance is slightly inferior to that of the optimal ML receiver but at a significantly reduced computational complexity.

This paper is organized as follows. A single-carrier communications system under the effect of radar interference of various power levels is investigated in Section II. Section III presents an OFDM-based multi-carrier communications receiver in the presence of radar signal as well as its detection schemes, and the error rate performance analysis of various decoders. Section IV concludes the paper.

II. Single-Carrier Communication System

First we look at a single-carrier communications system affected by a radar interference, which is a special case of the OFDM-based multi-carrier communications receiver analyzed in Section III but for which analytical evaluations are more tractable. In this section, we analytically derive the optimal ML detection scheme then present the error rate expressions for optimal and suboptimal decoders. Finally, we design signal constellations for two different optimization problems: (a) to maximize the transmission rate under average power and error rate constraints, and (b) to minimize the probability of error under a certain power budget and a fixed rate condition.

A. System Model and Detection Schemes

Radar systems periodically transmit pulses of large amplitude[1] and short duration, while communications systems generally send signals of significantly lower power, smaller bandwidth, and 100% duty-cycle. This implies that a narrowband communications system experiences the radar interference as an approximately amplitude-constant additive signal. This amplitude can be accurately estimated by, for example, listening periodically to the channel for some time prior to transmission, which is doable because of the slowly varying parameters of the radar system. The phase shift, on the other hand, is from the multiplication of the radar carrier frequency by the radar pulse propagation delay; even a small variation in propagation delay causes a large phase difference, which may be difficult to track; for this reason and similar to well accepted fading models [21], the phase is assumed unknown and uniformly distributed on $[0, 2\pi]$. This assumption is consistent with [19], which shows that the joint distribution of the radar amplitude and phase consists of a union of multiple constant amplitudes, uniform phase pieces. In other words, for several amplitudes, the joint distribution of the radar interference amplitude and phase is uniformly distributed across the phase (for each given amplitude); moreover, one of the amplitudes clearly dominates the others. In the following single-carrier system, we thus approximate the radar interference at the communications receiver as an additive signal with known amplitude and unknown uniform phase.

The discrete-time complex-valued received signal at the single-carrier communications receiver is

$$Y = \sqrt{\mathsf{S}}X + \sqrt{\mathsf{I}}e^{j\Theta} + Z, \tag{1}$$

where X is the transmitted symbol from the constellation $\mathcal{X} = \{x_1, \ldots, x_M\}$ of unit-energy and equally-likely points,

[1]Since the radar power is significantly higher than the communications power, the analog-to-digital converter at the communications receiver might not see the small communications signal. This may be an issue in practice, but can be mitigated [20]. Note that mitigating this effect is not the focus of this work.

Θ is the radar phase uniform in $[0, 2\pi)$, and Z is a zero-mean unit-variance proper-complex Gaussian noise. The random variables (X, Θ, Z) are mutually independent. S denotes the average Signal-to-Noise Ratio (SNR) of the communications signal, while I denotes the average Interference-to-Noise Ratio (INR) of the radar interference. The pair (S, I) are assumed known and fixed at the communications receiver.

For this single-carrier system, we have adopted the standard narrow-band frequency-flat slowly-varying fading model, and thus assumed that the channel gain $(\sqrt{\mathsf{S}})$ is known (i.e., has been accurately estimated via pilot tones) at the receiver. The probabilities of error are reported next for a fixed S. For time-varying channels, one should average the error rate expressions derived in this paper over the assumed statistics for S. As detailed later in Section III, the joint distribution of the radar amplitude and phase can be approximated by a single dominant amplitude and a uniform phase for many different radar pulse shapes; for this reason, if the channel between the radar transmitter and the communications receiver distorts the radar waveform, such a distortion only causes the value of the dominant amplitude to change; the assumption in this work is that the power of such a dominant amplitude (I) can be accurately estimated and thus can be assumed known at the communications receiver. For time-varying channels, one should average the error rate expressions derived in this paper over the assumed statistics for I.

Based on the above listed assumptions, the distribution of the channel output Y in (1) conditioned on the transmitted communications symbol X and the radar phase Θ is

$$f_{Y|X,\Theta}(y|x,\theta) = \frac{e^{-|y-\sqrt{\mathsf{S}}x-\sqrt{\mathsf{I}}e^{j\theta}|^2}}{\pi}, \quad y, x \in \mathbb{C},\ \theta \in [0, 2\pi). \tag{2}$$

Since the radar phase is unknown, the channel output conditional distribution is

$$\begin{aligned} f_{Y|X}(y|x) &= \mathbb{E}_\Theta[f_{Y|X,\Theta}(y|x,\theta)] \\ &= \frac{1}{2\pi}\int_0^{2\pi} \frac{1}{\pi} e^{-|y-\sqrt{\mathsf{S}}x|^2-\mathsf{I}+2\Re\{(y-\sqrt{\mathsf{S}}x_\ell)\sqrt{\mathsf{I}}e^{-j\Theta}\}} d\theta \\ &= \frac{1}{\pi} e^{-|y-\sqrt{\mathsf{S}}x|^2-\mathsf{I}} I_0\big(2\sqrt{\mathsf{I}}|y-\sqrt{\mathsf{S}}x_\ell|\big), \end{aligned} \tag{3}$$

where the equality in (3) follows from the definition of I_0, the modified Bessel function of the first kind of order zero [22, eq. (9.6.16)].

The optimal ML decoder for the channel in (3) chooses an estimate of the transmitted symbol $x_\ell \in \mathbb{C}$

$$\begin{aligned} \hat{\ell}^{(\text{OPT})}(y) &= \arg\max_{\ell\in[1:M]} f_{Y|X}(y|x_\ell) \\ &= \arg\min_{\ell\in[1:M]} \Big(|y-\sqrt{\mathsf{S}}x_\ell|^2 - \ln I_0\big(2\sqrt{\mathsf{I}}|y-\sqrt{\mathsf{S}}x_\ell|\big)\Big). \end{aligned} \tag{4}$$

We next thoroughly investigate two regimes for the decoder in (4): weak radar interference when the INR is low compared to the SNR, and (very) strong radar interference when the INR is (much) higher than the SNR.

1) Low INR Regime: When $\mathsf{I} \ll \mathsf{S}$, from [22, eq. (9.6.12)], we have $I_0(z) \cong 1$ for $|z| \ll 1$ in (4). As a result, the optimal ML decoder in (4) can be approximated as

$$\hat{\ell}^{(\text{OPT})}(y) \cong \arg\min_{\ell\in[1:M]} |y-\sqrt{\mathsf{S}}x_\ell|^2 =: \hat{\ell}^{(\text{TIN})}(y). \tag{5}$$

We can see that the decoder at low INR is actually the minimum Euclidean distance decoder implying that the radar interference is treated as Gaussian noise at low INR. We refer to the decoder in (5) as the 'TIN' decoder, in which 'TIN' stands for Treat Interference as Noise.

2) High INR Regime: When $\mathsf{I} \gg \mathsf{S}$, from [22, eq. (9.7.1)], we have $I_0(z) \cong e^{|z|}$ for $|z| \gg 1$ in (4). As a result, the optimal ML decoder in (4) can be approximated as

$$\hat{\ell}^{(\text{OPT})}(y) \cong \arg\min_{\ell\in[1:M]} \Big(|y-\sqrt{\mathsf{S}}x_\ell| - \sqrt{\mathsf{I}}\Big)^2 =: \hat{\ell}^{(\text{IC})}(y). \tag{6}$$

We refer to the decoder in (6) as the 'IC' decoder, in which 'IC' stands for Interference Cancellation.

B. Decision Regions

In this section we take a closer look at the decoding regions of the optimal (ML) and suboptimal (TIN and IC) detection schemes to get a better visualization of differences between having only Gaussian noise and having both Gaussian noise and radar interference.

Optimal ML receiver in (4): point x_ℓ is preferred to x_k if

$$\begin{aligned} &|y-\sqrt{\mathsf{S}}x_\ell|^2 - \ln I_0\big(2\sqrt{\mathsf{I}}|y-\sqrt{\mathsf{S}}x_\ell|\big) \\ &\qquad < |y-\sqrt{\mathsf{S}}x_k|^2 - \ln I_0\big(2\sqrt{\mathsf{I}}|y-\sqrt{\mathsf{S}}x_k|\big). \end{aligned} \tag{7}$$

1) Low INR Regime: For $\mathsf{I} \ll \mathsf{S}$, the TIN receiver in (5) prefers point x_ℓ to x_k if

$$|y-\sqrt{\mathsf{S}}x_\ell|^2 < |y-\sqrt{\mathsf{S}}x_k|^2. \tag{8}$$

In other words, the TIN receiver decodes x_ℓ if the received signal y is closer in Euclidean distance to x_ℓ than x_k, as in the AWGN-only channel.

2) High INR Regime: For $\mathsf{I} \gg \mathsf{S}$, the IC receiver in (6) prefers point x_ℓ to x_k if

$$\Big(|y-\sqrt{\mathsf{S}}x_\ell| - \sqrt{\mathsf{I}}\Big)^2 < \Big(|y-\sqrt{\mathsf{S}}x_k| - \sqrt{\mathsf{I}}\Big)^2. \tag{9}$$

Let $d_{y,\ell} := |y-\sqrt{\mathsf{S}}x_\ell|$ be the Euclidean distance between the received signal y and the constellation point x_ℓ. The expression in (9), which is no longer a minimum Euclidean distance decoder, can be separated into the following cases:

Case 1: $\left.\begin{matrix} |y-\sqrt{\mathsf{S}}x_\ell| > \sqrt{\mathsf{I}} \\ |y-\sqrt{\mathsf{S}}x_k| > \sqrt{\mathsf{I}} \end{matrix}\right\}$ if $d_{y,\ell} < d_{y,k}$ (i.e. y is closer to x_ℓ);

Case 2: $\left.\begin{matrix} |y-\sqrt{\mathsf{S}}x_\ell| > \sqrt{\mathsf{I}} \\ |y-\sqrt{\mathsf{S}}x_k| \le \sqrt{\mathsf{I}} \end{matrix}\right\}$ if $\dfrac{d_{y,\ell}+d_{y,k}}{2} < \sqrt{\mathsf{I}}$;

Case 3: $\left.\begin{matrix} |y-\sqrt{\mathsf{S}}x_\ell| \le \sqrt{\mathsf{I}} \\ |y-\sqrt{\mathsf{S}}x_k| > \sqrt{\mathsf{I}} \end{matrix}\right\}$ if $\dfrac{d_{y,\ell}+d_{y,k}}{2} \ge \sqrt{\mathsf{I}}$;

Case 4: $\left.\begin{matrix} |y-\sqrt{\mathsf{S}}x_\ell| \le \sqrt{\mathsf{I}} \\ |y-\sqrt{\mathsf{S}}x_k| \le \sqrt{\mathsf{I}} \end{matrix}\right\}$ if $d_{y,\ell} \ge d_{y,k}$ (i.e. y is further from x_ℓ).

In other words, the shape of a decoding region depends on the minimum Euclidean distance (case 1), the maximum Euclidean

TABLE I

THE OPTIMAL AND SUBOPTIMAL IC DECODING REGIONS FOR 8-PSK AT $S_{dB} = 10$ IN DIFFERENT REGIMES

I_{dB} \ Decoders	ML	IC
$I_{dB} = 2.5$ ($I \ll S$)	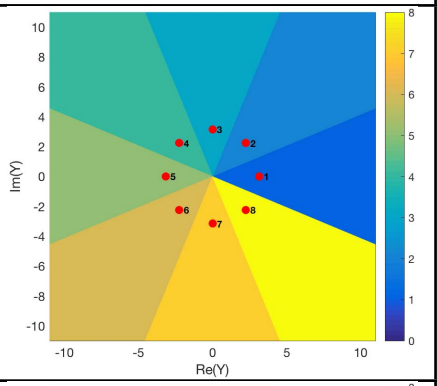	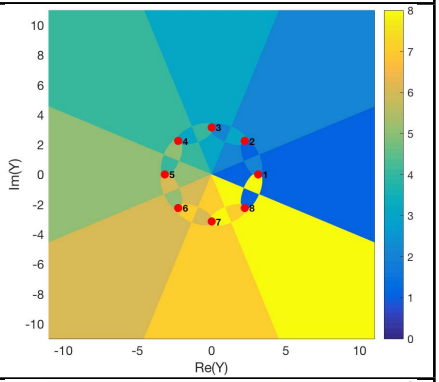
$I_{dB} = 10$ ($I \cong S$)	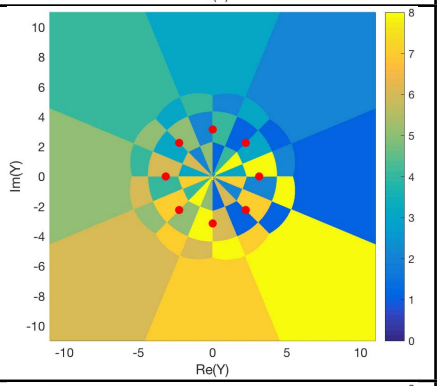	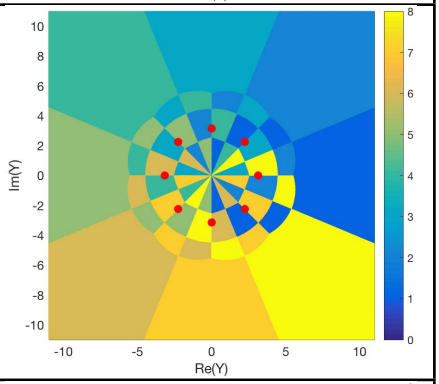
$I_{dB} = 15$ ($I \gg S$)	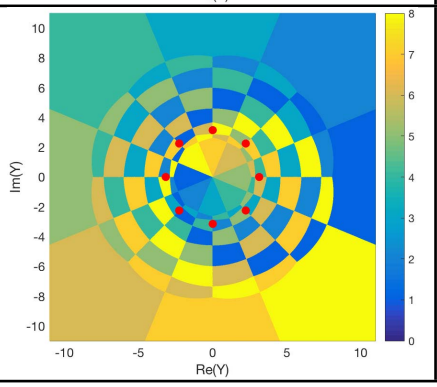	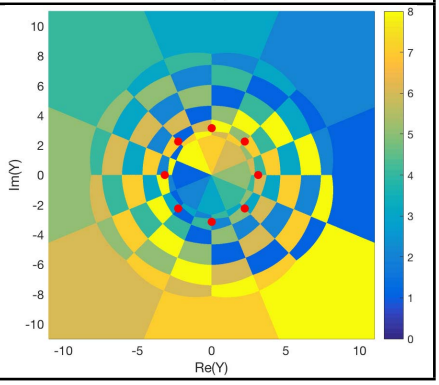

distance (case 4), or the average distances (cases 2 and 3) that cause "sliced areas" as seen later in Table I. Hence, the IC decoder produces decoding regions that spread across multiple disjoint subsets of $\mathbb{C}$, rather than being the Voronoi region of a constellation point (as for the TIN decoder).

Table I shows the optimal and suboptimal decoding regions for an 8-PSK constellation at $S_{dB} = 10$ dB for different INR's. The red bullets represent a constellation point numbered from 1 to 8. The decoding regions of the TIN decoder are the same as the optimal ML decoding regions at $I_{dB} = 0.25$ and do not depend on the INR. For the AWGN ($I = 0$) case, all decoders yield exactly the same decoding regions, based on the minimum distance only. At low INR ($I_{dB} = 0.25S_{dB}$), the decoding regions of the IC decoder shows visual differences compared with those of the optimal one. At mid INR ($I_{dB} = S_{dB}$), the IC decoder produces similar shapes (but slightly larger) as the optimal ML decoder. At high INR ($I_{dB} = 1.5S_{dB}$), the IC decoding regions are almost identical as the optimal ML ones.

Based on these results, we expect the TIN decoder to be very good at low INR ($I \ll S$); as I increases, the optimal decoding regions spread to other regions and the IC decoder should be better than the TIN decoder at mid INR ($I \cong S$); as I further increases much higher than S, the IC decoder should be very good and approach the performance of the optimal one at high INR ($I \gg S$). This intuition is next formalized.

C. Symbol Error Rate (SER) Analysis

We analyze the SER of the suboptimal TIN (in (5)) and IC (in (6)) decoders at low and high INR.

Low INR Regime: The probability of error of the optimal ML decoder is upper bounded by that of the TIN decoder as

$$\begin{aligned} &P_{\mathrm{e}}^{(\mathrm{OPT})} \\ &\leq P_{\mathrm{e}}^{(\mathrm{TIN})} \\ &= \frac{1}{M}\sum_{\ell=1}^{M}\mathbb{P}\left[|Y-\sqrt{\mathsf{S}}x_\ell|^2 > \min_{k:k\neq\ell}|Y-\sqrt{\mathsf{S}}x_k|^2\Big|X=x_\ell\right] \\ &= \frac{1}{M}\sum_{\ell=1}^{M}\mathbb{P}\left[\Re\left\{(\sqrt{\mathsf{I}}e^{j\Theta}+Z)e^{-j\angle(x_k-x_\ell)}\right\} > \frac{\sqrt{\mathsf{S}}d_{k,\ell}}{2}\exists k\neq\ell\right] \\ &\leq \frac{1}{M}\sum_{\substack{(\ell,k)\in[M]^2\\ k\neq\ell}}\mathbb{P}\left[\Re\left\{(\sqrt{\mathsf{I}}e^{j\Theta}+Z)e^{-j\angle(x_k-x_\ell)}\right\} > \frac{\sqrt{\mathsf{S}}d_{k,\ell}}{2}\right] \end{aligned} \tag{10}$$

$$\approx N_{\min}\mathbb{E}_\Theta\left[Q\left(\sqrt{\frac{\mathsf{S}d_{\min}^2}{2}}-\sqrt{2\mathsf{I}}\cos(\Theta)\right)\right], \tag{11}$$

where (10) follows by the union bound. The expression in (10) no longer depends on $\angle(x_k - x_\ell)$ because for a circularly symmetric random variable Z and an angle ϕ, we have $Ze^{-j\phi} \sim Z$, and for a uniformly distributed random variable Θ and an angle ϕ, we have $\cos(\Theta+\phi) \sim \cos(\Theta)$; therefore, this expression is only a function of $d_{k,\ell} := |x_k - x_\ell|$. Finally in (11), we have defined $d_{\min} := \min_{k:k\neq\ell} d_{k,\ell}$ and $N_{\min}$ as the average number of nearest neighbors. The approximation in (11) is usually referred to as the Nearest Neighbor Union Bound (NNUB) [23] and is tight at high SNR. The approximation in (11) can be made a firm upper bound on $P_{\mathrm{e}}^{(\mathrm{TIN})}$ by replacing $N_{\min}$ with $M-1$.

High INR Regime: The probability of error of the optimal ML decoder is upper bounded by that of the IC decoder as

$$\begin{aligned} P_{\mathrm{e}}^{(\mathrm{OPT})} \quad &\leq \quad P_{\mathrm{e}}^{(\mathrm{IC})} = \frac{1}{M}\sum_{\ell=1}^{M}\mathbb{P}\left[\left(|y-\sqrt{\mathsf{S}}x_\ell|-\sqrt{\mathsf{I}}\right)^2\right. \\ &\qquad \left.> \min_{k:k\neq\ell}\left(|y-\sqrt{\mathsf{S}}x_k|-\sqrt{\mathsf{I}}\right)^2\Big|X=x_\ell\right] \\ &\overset{\mathsf{I}\gg\mathsf{S}\gg 1}{\approx} \frac{1}{M}\sum_{\ell=1}^{M}\mathbb{P}\left[Z_{\mathrm{eq}}\mathrm{sign}\left(r_k(\Theta)-r_\ell(\Theta)\right)\right. \\ &\qquad \left.> \frac{\sqrt{\mathsf{S}}|r_k(\Theta)-r_\ell(\Theta)|}{2}\exists k\neq\ell\right] \\ &= \quad \frac{1}{M}\sum_{\ell=1}^{M}\mathbb{E}_\Theta\left[Q\left(\Delta_{k,\ell}^{+}(\Theta)\right)+Q\left(\Delta_{k,\ell}^{-}(\Theta)\right)\right], \end{aligned} \tag{12}$$

where, based on the derivations in Appendix A, we have

$$r_\ell(\Theta) := \Re\{e^{-j\Theta}x_\ell\} \quad \forall\ell\in[1:M],\ Z_{\mathrm{eq}}\sim\mathcal{N}_R(0,\frac{1}{2}), \tag{13}$$

$$\Delta_{k,\ell}^{+}(\Theta) := \min_{\substack{k:k\neq\ell\\ \mathrm{sign}(r_k(\Theta)-r_\ell(\Theta))\geq 0}}\sqrt{\frac{\mathsf{S}}{2}}\left|r_k(\Theta)-r_\ell(\Theta)\right|, \tag{14}$$

$$\Delta_{k,\ell}^{-}(\Theta) := \min_{\substack{k:k\neq\ell\\ \mathrm{sign}(r_k(\Theta)-r_\ell(\Theta))< 0}}\sqrt{\frac{\mathsf{S}}{2}}\left|r_k(\Theta)-r_\ell(\Theta)\right|. \tag{15}$$

We note that the approximation in (12) does not have a simple interpretation as (11) in terms of geometric properties of the constellation; it is, however, easy to evaluate numerically.

Next, we analyze the SER expressions in (11) and (12) for commonly-used signal constellations.

1) Pulse-Amplitude Modulation (PAM):

a) Low INR Regime: For $\mathsf{I} < \mathsf{S}$, the error probability of the TIN decoder in (11) is

$$P_{\mathrm{e,PAM}}^{(\mathrm{ML})} \leq P_{\mathrm{e,PAM}}^{(\mathrm{TIN})} \approx 2\left(1-\frac{1}{M}\right) \times \mathbb{E}_\Theta\left[Q\left(\sqrt{\frac{6\mathsf{S}}{M^2-1}}-\sqrt{2\mathsf{I}}\cos(\Theta)\right)\right],$$

where the term $2\left(1-\frac{1}{M}\right)$ is the average number of nearest neighbors and $\sqrt{\frac{12}{M^2-1}}$ the minimum distance of an M-PAM.

b) High INR Regime: For $\mathsf{I} \gg \mathsf{S}$, the error probability of the IC decoder in (12), by the NNUB applied to (12), is

$$P_{\mathrm{e,PAM}}^{(\mathrm{ML})} \leq P_{\mathrm{e,PAM}}^{(\mathrm{IC})} \overset{\mathsf{I}\gg\mathsf{S}\gg 1}{\approx} 2\left(1-\frac{1}{M}\right) \times \mathbb{E}_\Theta\left[Q\left(\sqrt{\frac{6\mathsf{S}}{M^2-1}\cos^2(\Theta)}\right)\right],$$

whose derivation can be found in Appendix B.

2) Square Quadrature Amplitude Modulation (QAM):

a) Low INR Regime: For $\mathsf{I} < \mathsf{S}$, the error probability of the TIN decoder in (11) is

$$P_{\mathrm{e,QAM}}^{(\mathrm{ML})} \leq P_{\mathrm{e,QAM}}^{(\mathrm{TIN})} \approx 4\left(1-\frac{1}{\sqrt{M}}\right) \times \mathbb{E}_\Theta\left[Q\left(\sqrt{\frac{3\mathsf{S}}{M-1}}-\sqrt{2\mathsf{I}}\cos(\Theta)\right)\right],$$

where the term $4\left(1-\frac{1}{\sqrt{M}}\right)$ is the average number of nearest neighbors and $\sqrt{\frac{6}{M-1}}$ the minimum distance of an M-QAM.

b) High INR Regime: For $\mathsf{I} \gg \mathsf{S}$, the error probability of the IC decoder is given by (12) as the functions $\Delta_{k,\ell}^{\pm}(\Theta)$ in (14)-(15) cannot be expressed in simple terms for the M-QAM but can be done numerically.

3) Phase-Shift Keying (PSK):

a) Low INR Regime: For $\mathsf{I} < \mathsf{S}$, the error probability of the TIN decoder in (11) is

$$P_{\mathrm{e,PSK}}^{(\mathrm{ML})} \leq P_{\mathrm{e,PSK}}^{(\mathrm{TIN})} \approx 2\mathbb{E}_\Theta\left[Q\left(\sqrt{2\mathsf{S}}\sin\left(\frac{\pi}{M}\right)-\sqrt{2\mathsf{I}}\cos(\Theta)\right)\right],$$

where 2 is the average number of nearest neighbors and $2\sin\left(\frac{\pi}{M}\right)$ the minimum distance for an M-PSK.

b) High INR Regime: For $\mathsf{I} \gg \mathsf{S}$, the error probability of the IC decoder is given by (12) as the functions $\Delta_{k,\ell}^{\pm}(\Theta)$ in (14)-(15) cannot be expressed in simple terms for the M-PSK but can be numerically evaluated.

With these SER approximations for commonly-used constellations, we can then compare the performance of various decoders in terms of error rates.

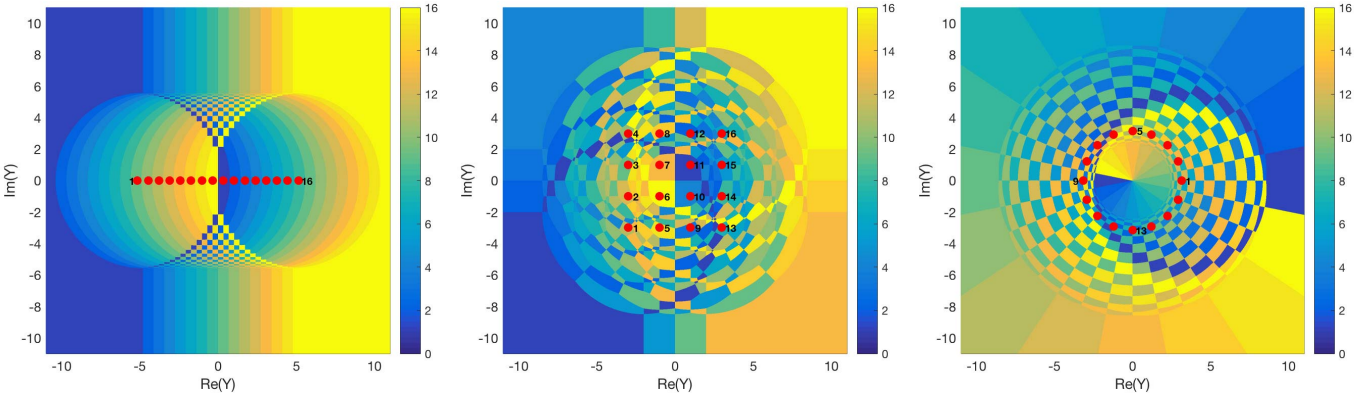

(a) 16-PAM: Optimal decoding regions. (b) 16-QAM: Optimal decoding regions. (c) 16-PSK: Optimal decoding regions.

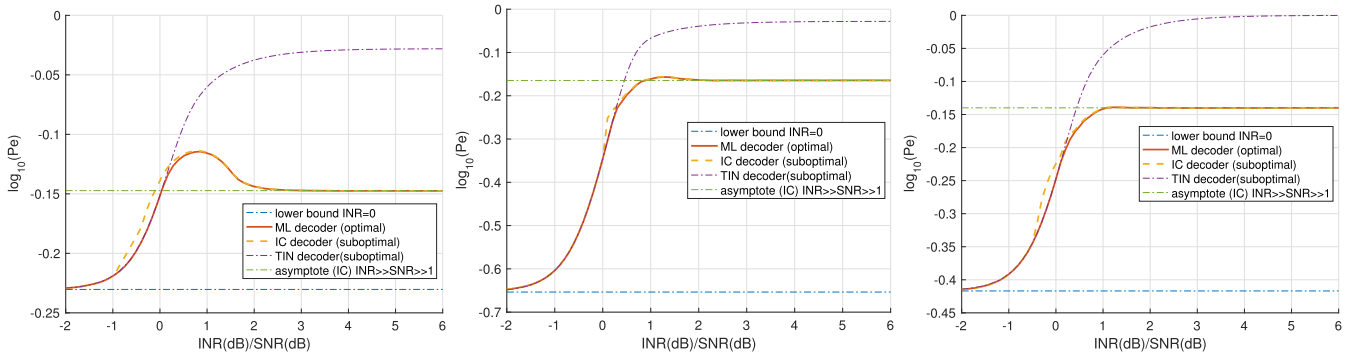

(d) 16-PAM: SER vs I in dB, for fixed S. (e) 16-QAM: SER vs I in dB, for fixed S. (f) 16-PSK: SER vs I in dB, for fixed S.

Fig. 1. Top: Optimal decoding regions for $\mathsf{S} = 10$ dB and $\mathsf{I} = 15$ dB. Bottom: SER vs I for $\mathsf{S} = 10$ dB.

D. SER Performance Evaluations

Here we report the optimal decoding regions and SER performance for the 16-PAM, 16-QAM, and 16-PSK constellations. The optimal decoding regions at $\mathsf{S} = 10$ dB and $\mathsf{I} = 15$ dB are at the top of Fig. 1, and the red bullets denote the constellation points numbered from 1 to 16. The SER curves are plotted against the INR (in dB) normalized by a fixed SNR of 10 dB at the bottom of Fig. 1. The lowest SER is at $\mathsf{I} = 0$ corresponding to the AWGN-only channel. The SER increases with INR (while keeping the SNR fixed) until it reaches its highest value at around $\mathsf{I}_{\text{dB}}/\mathsf{S}_{\text{dB}} \cong 1$; then it decreases and flattens out to an asymptote given by the SER expression in (12) in the limit for $\mathsf{I} \to \infty$. As expected, the TIN decoder provides an excellent approximation for the performance of the optimal ML decoder at low INR while the IC decoder does not perform as well in general in this regime. The opposite holds for high INR where the IC decoder is not much off compared to the optimal decoder–unexpectedly, even for low INR. We have normalized the (varying) I_{dB} by the (fixed) S_{dB} to highlight that the highest error rate occurs at SNR $\cong$ INR. Similar plots can be obtained by fixing different values of SNR (See Fig. 3(a) in Appendix C for more details).

E. Signal Constellation Design

Given the performance of commonly used constellations designed for the AWGN-only channel, a natural question is whether constellations optimized for the channel in (4) would have different shapes and properties. Here we are interested in designing two-dimensional signal constellations so as to optimize the communications system performance in the presence of a radar signal. We look at two optimization problems: (1) maximize the transmission rate, and (2) minimize the error rate. The performance comparison between the designed constellations and the commonly-used ones is presented later.

1) Optimization Formulation for Maximizing the Transmission Rate: Our goal is to design a constellation with the largest rate (i.e., number of points M) subject to a given average SER and average power constraints. Mathematically, for some desired maximum SER value of ε, we aim to determine

$$M^{(\text{OPT})}(\varepsilon) := \max \ M \tag{16}$$

$$\text{s.t. } \mathcal{X} = \{x_1, \cdots, x_M\}, \tag{16a}$$

$$P_{\text{e}}(\mathcal{X}) \le \varepsilon, \tag{16b}$$

$$\frac{1}{M}\sum_{\ell=1}^{M} |x_\ell|^2 \le 1, \quad x_\ell \in \mathbb{C}, \tag{16c}$$

where $P_{\text{e}}(\mathcal{X})$ is the SER approximation of the optimal ML decoder for the constellation $\mathcal{X}$ in (16a), and is given by (11) at low INR and (12) at high INR. This implies that the location of the constellation points in (16a) has to be optimized to satisfy the constraints for the average SER in (16b) and average power in (16c).

In our optimization algorithm, we start by fixing the number of points M (as small as 2) and find such a signal constellation that minimizes the SER approximations of the optimal

TABLE II
DESIGNED CONSTELLATIONS WITH MAXIMUM TRANSMISSION RATES AT VARIOUS S_{dB} AND $\mathsf{I}_{\mathrm{dB}} = 0.25\mathsf{S}_{\mathrm{dB}}$

S_{dB} \ ε	10^{-3}	10^{-5}	10^{-6}
15	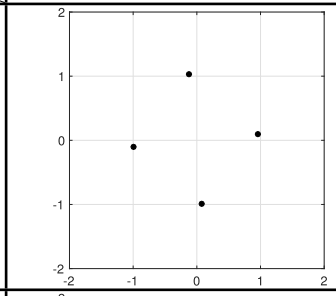	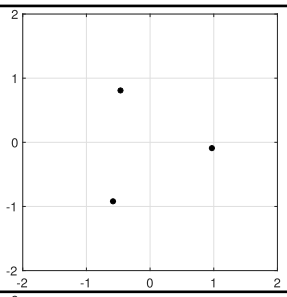	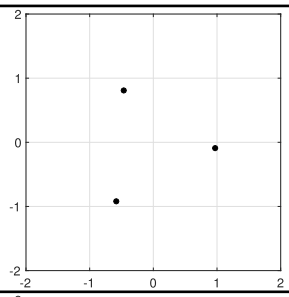
20	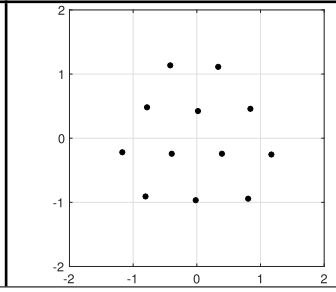	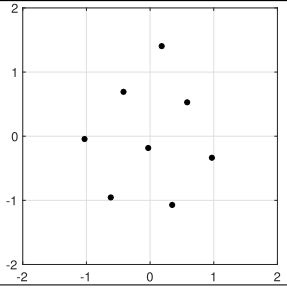	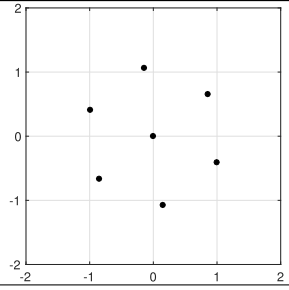

decoder; if the SER for the found constellation satisfies (16b) then we increase M by 1 and repeat these steps until the maximum SER requirement is violated. We then obtain the constellation with largest $M^{(\mathrm{OPT})}$ under the given constraints.

2) Optimization Formulation for Minimizing the Error Rate: Here we consider the problem of the constellation design that minimizes the SER subject to fixed rate (constellation size) and power constraints

$$P_{\mathrm{e}}^{(\mathrm{OPT})}(M) = \min \; P_{\mathrm{e}}(\mathcal{X}) \tag{17}$$

$$\text{s.t. } \mathcal{X} = \{x_1, \cdots, x_M\}, \tag{17a}$$

$$\frac{1}{M}\sum_{\ell=1}^{M} |x_\ell|^2 \leq 1, \quad x_\ell \in \mathbb{C}. \tag{17b}$$

In our optimization algorithm, we fix the constellation size M and find such a signal constellation that minimizes the SER approximations of the optimal decoder within a power budget.

We note that in both (non-convex) optimization problems, we use the numerical Global Search (GS) method in [24], which is available in the MATLAB Global Optimization Toolbox. GS is a gradient-based algorithm that uses a scatter-search mechanism to generate multiple randomized start points then analyzes and rejects the points that are unlikely to improve the best local minimum found so far. GS attempts to find the function's global minima by finding and comparing different local minima of smooth nonlinear optimization problem; thus, the results are not always guaranteed to be globally optimal. In order to minimize the chance of having found a local optimum, we run the GS method multiple times with different start points as well as other parameters.

3) Optimization Results for Constellations With Maximal Rate: We show here the results from the optimization problem in Subsection II-E1, where we aim to design a complex-valued constellation that can achieve the largest number of points $M^{(\mathrm{OPT})}$ subject to average power and error rate constraints.

Table II reports the designed constellations with maximum number of points for fixed ε of 10^{-3}, 10^{-5}, and 10^{-6}, at $\mathsf{S}_{\mathrm{dB}} = 15$ and 20, and $\mathsf{I}_{\mathrm{dB}} = 0.25\mathsf{S}_{\mathrm{dB}}$. We observe that a triangle is initially formed with just 3 points then more points are added to form more triangles next to one another. At $\varepsilon = 10^{-6}$ and $\mathsf{S}_{\mathrm{dB}} = 20$, the designed constellation of $M = 7$ looks like a hexagon with a center point. As we relax the SER requirements to allow for more transmitted points, we observe that the designed constellations are shaped as concentric hexagons with multiple layers; for example, only 8 points are allowed for transmission for the SER constraint of $\varepsilon = 10^{-5}$ while 12 points can be sent for $\varepsilon = 10^{-3}$. Generally, the shape of the designed constellation tends to a hexagonal lattice (the best packing in two dimensions) as M increases.

Table III reports the designed constellations with maximum number of points for fixed ε of $10^{-0.82}$, $10^{-1.15}$, and $10^{-1.48}$, at $\mathsf{S}_{\mathrm{dB}} = 20$ and 30, and $\mathsf{I} = 2\mathsf{S}_{\mathrm{dB}}$. To obtain various values of $M^{(\mathrm{OPT})}(\varepsilon)$, the SER constraints are set relatively high due to the SNRs used in our example (see Fig. 3(b) in Appendix C for a discussion on the SNR requirement subject to an SER constraint). We observe that the designed constellations are shaped as unequally-spaced PAMs. The intuition is that the points are placed as far apart from one another as possible (given the power constraint) so as to result in larger possible minimum distances. As proved in Appendix A, the channel at high INR is equivalent to the real-valued phase-fading channel (see (43)) so it makes sense that the points are placed according to the optimal packing in one dimension (at least at high SNR), which is the equi-lattice (equally-spaced points on a straight line). Note that our optimization algorithm returns an optimized constellation, but any rotation of it is also optimal; in other words, the optimal constellation is unique up to a phase rotation, as long as this rotation is known at the receiver. Thus, for sake of presentation, we aligned the designed constellations to the 'in-phase' axis of the figures.

TABLE III

DESIGNED CONSTELLATIONS WITH MAXIMUM TRANSMISSION RATES AT VARIOUS S_{dB} AND $\mathsf{I}_{\mathrm{dB}} = 2\mathsf{S}_{\mathrm{dB}}$

S_{dB} \ ε	$10^{-0.82}$	$10^{-1.15}$	$10^{-1.48}$
20	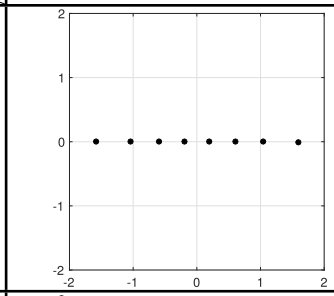	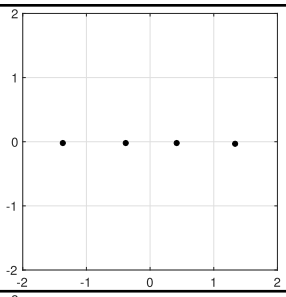	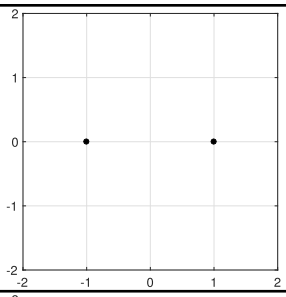
30	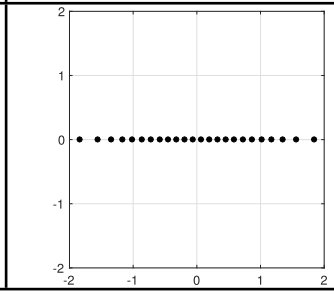	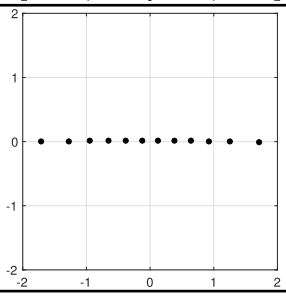	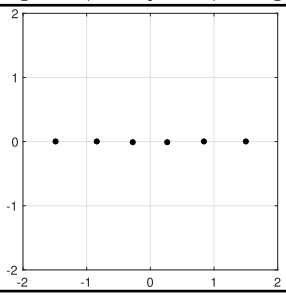

4) Optimization Results for Constellations With Minimum Error Rate: We show here the results from the optimization problem in Subsection II-E2, where we aim to design a complex-valued constellation that can yield the lowest SER under average power and fixed constellation size constraints.

Table IV reports the designed constellations with minimum symbol error rates for fixed number of points M in $\{4,8,16\}$, at $\mathsf{S}_{\mathrm{dB}} = 20$, and for different values $\mathsf{I}_{\mathrm{dB}}/\mathsf{S}_{\mathrm{dB}}$. We observe that the optimized constellation tends to shape like a concentric hexagon when $\mathsf{I} \ll \mathsf{S}$, while it tends to shape like a unevenly PAM when $\mathsf{I} \gg \mathsf{S}$. Notice that the shapes of the designed constellations for minimizing the error rates are similar to those of the complimentary problem of maximizing the transmission rates. We heuristically observe that the highest SER takes place in the range of INR's close to SNR. We expect to see a transitioning between a hexagonal constellation at low INR and a PAM-like one at high INR around $\mathsf{I} \cong \mathsf{S}$. However, the exact value of $\frac{\mathsf{I}_{\mathrm{dB}}}{\mathsf{S}_{\mathrm{dB}}}$ where the transitioning occurs depends on the SNR, modulation scheme and constellation size. The values of $\frac{\mathsf{I}_{\mathrm{dB}}}{\mathsf{S}_{\mathrm{dB}}}$ used in Table IV were numerically chosen to highlight this transition, in particular, we chose $\mathsf{I}_{\mathrm{dB}} = 20, 25,$ and 28 for $M = 4, 8,$ and 16, respectively.

5) Performance Comparison: We compare here the performance, in terms of transmission and error rates, of the designed constellations with the classical ones. Numerical results show that our designed constellations outperform the others.

Table V compares the largest transmission rate of the designed constellations with the practical ones, which are PAM and PSK in our example, subject to the SER upper bounded by $\varepsilon = 10^{-1}$ at $\mathsf{S}_{\mathrm{dB}} = 10, 15,$ and 20 for low INR, and $\mathsf{S}_{\mathrm{dB}} = 10, 20,$ and 30 for high INR. At low INR ($\mathsf{I}_{\mathrm{dB}} = 0.25\mathsf{S}_{\mathrm{dB}}$), the designed constellations achieve the largest rates. As I increases, less points can be sent. At high INR ($\mathsf{I}_{\mathrm{dB}} = 2\mathsf{S}_{\mathrm{dB}}$), the rates achieved by PSK and PAM are very competitive with the designed constellations. In these cases, the designed constellations have advantages of yielding a lower SER.

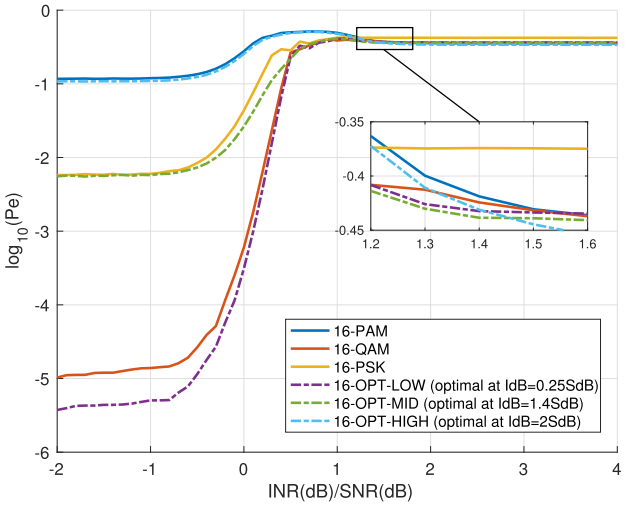

Fig. 2. SER Comparison for $M = 16$ and $\mathsf{S} = 20$ dB.

Fig. 2 shows the SER as a function of normalized $\frac{\mathsf{I}_{\mathrm{dB}}}{\mathsf{S}_{\mathrm{dB}}}$ for the designed constellations with $M = 16$ points at $\mathsf{S}_{\mathrm{dB}} = 20$ in Table IV. Note that those constellations were optimized for a fixed INR and may not be optimal for the whole INR range. For comparison, we report the SER for the 16-PAM, 16-QAM, and 16-PSK, as representatives of the practical constellations. At low INR, the classical 16-PAM, 16-QAM, and 16-PSK are markedly suboptimal; the best performance is attained by the 16-OPT-LOW, which was optimized for $\mathsf{I}_{\mathrm{dB}} = 0.25\mathsf{S}_{\mathrm{dB}} = 5$. At mid INR, the 16-OPT-MID, which was optimized for

TABLE IV

DESIGNED CONSTELLATIONS WITH MINIMUM SER AT $\mathsf{S}_{\mathrm{dB}} = 20$ AND $\mathsf{I}_{\mathrm{dB}} = 0.25\mathsf{S}_{\mathrm{dB}} = 5$, $\mathsf{I}_{\mathrm{dB}} \cong \mathsf{S}_{\mathrm{dB}} = 20$, AND $\mathsf{I}_{\mathrm{dB}} = 2\mathsf{S}_{\mathrm{dB}} = 40$ FOR $M = 4, 8$, AND 16

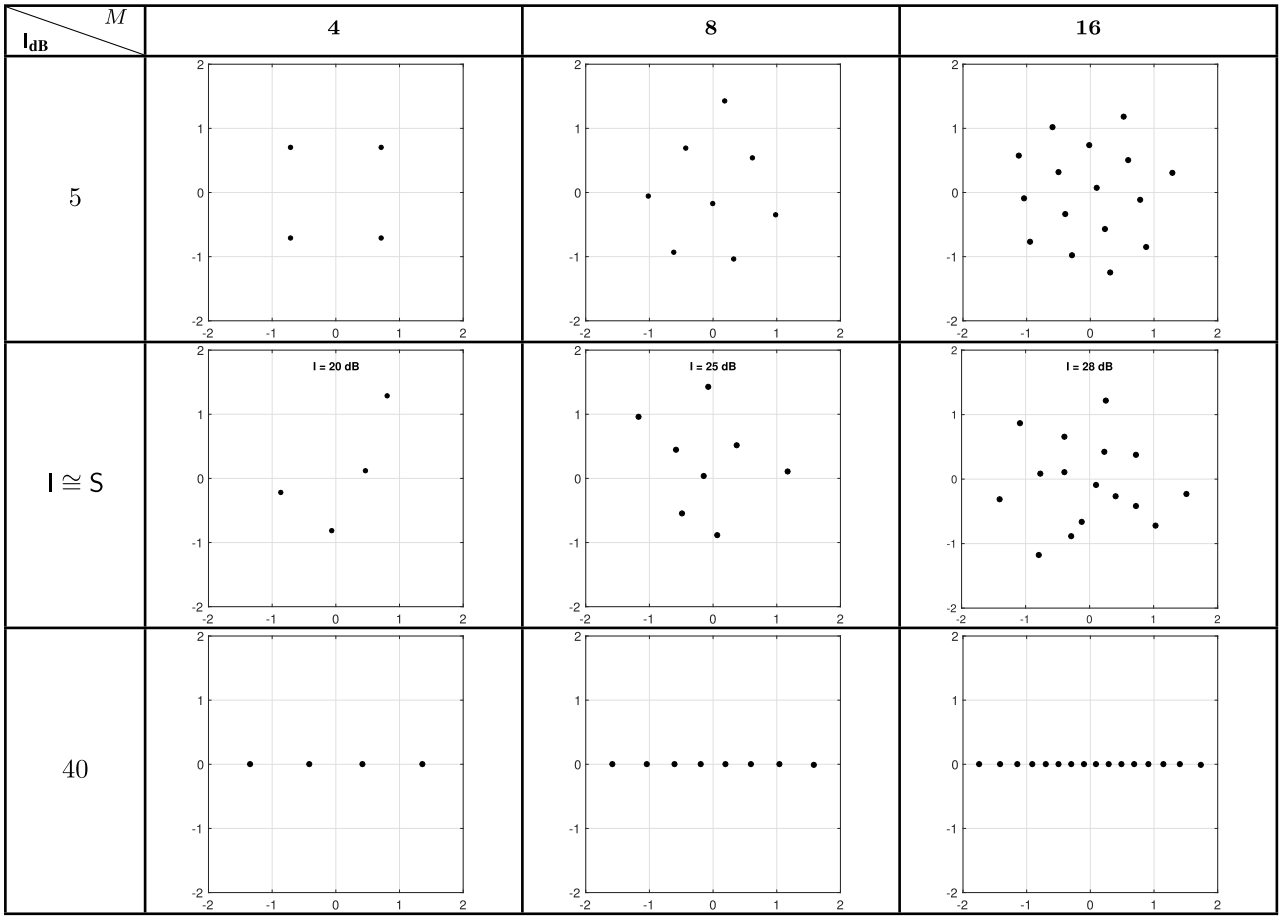

TABLE V

COMPARISON OF MAXIMUM M FOR DIFFERENT CONSTELLATIONS FOR $\varepsilon = 10^{-1}$

(a) TIN Decoder at various S_{dB} and $\mathsf{I}_{\mathrm{dB}} = 0.25\mathsf{S}_{\mathrm{dB}}$

Constellation \ S_{dB}	10	15	20
PAM	$M = 3$, $P_{\mathrm{e}} = 10^{-1.2210}$	$M = 5$, $P_{\mathrm{e}} = 10^{-1.0241}$	$M = 7$, $P_{\mathrm{e}} = 10^{-1.3020}$
PSK	$M = 4$, $P_{\mathrm{e}} = 10^{-1.3706}$	$M = 8$, $P_{\mathrm{e}} = 10^{-1.0835}$	$M = 13$, $P_{\mathrm{e}} = 10^{-1.1219}$
OPT	$M = 4$, $P_{\mathrm{e}} = 10^{-1.3725}$	$M = 11$, $P_{\mathrm{e}} = 10^{-1.0301}$	$M = 26$, $P_{\mathrm{e}} = 10^{-1.0562}$

(b) IC Decoder at various S_{dB} and $\mathsf{I}_{\mathrm{dB}} = 2\mathsf{S}_{\mathrm{dB}}$

Constellation \ S_{dB}	10	20	30
PAM	$M = 2$, $P_{\mathrm{e}} = 10^{-1.2377}$	$M = 5$, $P_{\mathrm{e}} = 10^{-1.0838}$	$M = 15$, $P_{\mathrm{e}} = 10^{-1.0290}$
PSK	$M = 2$, $P_{\mathrm{e}} = 10^{-1.2377}$	$M = 5$, $P_{\mathrm{e}} = 10^{-1.0020}$	$M = 11$, $P_{\mathrm{e}} = 10^{-1.0001}$
OPT	$M = 2$, $P_{\mathrm{e}} = 10^{-1.2377}$	$M = 5$, $P_{\mathrm{e}} = 10^{-1.0882}$	$M = 16$, $P_{\mathrm{e}} = 10^{-1.0192}$

$\mathsf{I}_{\mathrm{dB}} = 1.4\mathsf{S}_{\mathrm{dB}} = 28$ where the SER curve of the 16-OPT-LOW crosses that of the 16-OPT-HIGH, performs slightly better than 16-OPT-LOW and 16-OPT-HIGH. At high INR, the 16-PAM is very competitive with the 16-OPT-HIGH, which was optimized for $\mathsf{I}_{\mathrm{dB}} = 2\mathsf{S}_{\mathrm{dB}} = 40$.

At all range of INR, our optimally designed constellations outperform the practically-used ones in terms of SER. We thus conclude that one should send a hexagonal-like constellation in the low INR regime while a PAM constellation (as opposed to an optimized unevenly spaced PAM) in the high INR regime.

III. MULTI-CARRIER COMMUNICATION SYSTEM

Narrowband single carrier systems, such as those studied in the previous section, are no longer the physical layer choice for high speed networks. LTE, WiFi and foreseeably 5G are OFDM-based. In this section, we consider a general OFDM-based multi-carrier communications systems of N subcarriers and L OFDM blocks with additive white Gaussian noise and radar interference, as opposed to the single-carrier system where $N = L = 1$. Here we assume a frequency-selective channel with negligible Doppler such that all the

standard assumptions for OFDM systems (i.e., narrow-band flat-fading on each subcarrier, and free of inter-carrier interference) hold [21]. In the following, the channel is considered flat, static, and known on each sub-carrier; extensions to other fading models is left for future work.

A. System Model [19]

The OFDM-based communications system operates at a carrier frequency of f_C Hz with N subcarriers over a total bandwidth of B_C Hz. The transmitted communications signal consists of L OFDM symbols, each with a duration of T_C seconds. The pulsed radar system operates at a carrier frequency f_R Hz over a bandwidth of B_R Hz. The pulse repetition interval (PRI) of the radar pulse $w_R(t)$ is T_R seconds and each pulse has width of τ_R seconds. The radar signal is assumed to arrive at the OFDM receiver $\mathrm{T_d}$ seconds after the communications signal. This time delay $\mathrm{T_d}$ is unknown at the communications receiver and thus modeled as random. The communications receiver is assumed to sample in synchrony with the transmitted symbols, with the sampling period of $T_S = 1/B_C$ seconds, at the time instants $t = dT_S, d \in \mathbb{N}$. At the OFDM receiver, the discrete-time complex-valued baseband received signal is expressed as

$$\mathbf{Y} = \sqrt{\mathbf{S}}\mathbf{X} + \mathbf{I} + \mathbf{Z} \in \mathbb{C}^{N\times L}, \tag{18}$$

where

- $\mathbf{S} \in \mathbb{R}_+^{N\times N}$ is a diagonal matrix containing the average Signal-to-Noise Ratios of the communications signal for the corresponding subcarriers,
- $\mathbf{X} \in \mathbb{C}^{N\times L}$ is a matrix of the transmitted symbols drawn from the equally-likely complex-valued signal constellation $\mathcal{X} = \{x_1, \cdots, x_M\}$ with unitary average power,
- $\mathbf{I} \in \mathbb{C}^{N\times L}$ is a matrix of the radar interference with rows corresponding to the subcarriers and columns corresponding to the OFDM blocks. This matrix is a function of the random variable $\mathrm{N_d} := \lfloor \frac{\mathrm{T_d}}{\mathrm{T_S}} \rfloor$, which represents the time delay in samples (justification given later), and
- $\mathbf{Z} \in \mathbb{C}^{N\times L}$ is the proper-complex Gaussian noise, whose components are independent with zero mean and unit variance.

The random variables $(\mathbf{X}, \mathrm{N_d}, \mathbf{Z})$ are mutually independent. The matrix $\mathbf{S}$ is assumed fixed and known at the receiver.

The interference matrix $\mathbf{I}$ is obtained by passing the received radar signal through the OFDM receiver chain. After sampling, removing the cyclic prefix of length N_{CP} samples, and performing an N-point Discrete Fourier Transform (DFT), the received radar signal at the OFDM receiver on the $k^{\text{th}} \in [0 : N-1]$ subcarrier and $m^{\text{th}} \in [0 : L-1]$ OFDM block of the matrix $\mathbf{I}$ is given by (see [19] for detailed derivation)

$$I_{k,m} = \mathrm{DFT}\big(v_{R,m}[n] e^{j2\pi\Delta_f n T_S}, n \in [0 : N-1]\big)\, e^{j\psi_m} \tag{19}$$

where $v_{R,m}[n] := w_R\big((n + mN_C + N_{CP} - \mathrm{N_d})\, T_S\big)$ is the sampled version of the passband radar signal $w_R(t)$ during the m^{th} OFDM block, $N_C := \lceil \frac{T_C}{T_S} \rceil$ is the OFDM symbol duration in samples, $N_R := \lceil \frac{T_R}{T_S} \rceil$ is the pulse repetition interval of the radar signal in samples, $\Delta_f := f_R - f_C$ is the difference between the carrier frequencies of the two systems, and the radar phase at the m^{th} block is defined as

$$\psi_m := 2\pi T_S\big(\Delta_f(mN_C + N_{CP}) - f_R \mathrm{N_d}\big). \tag{20}$$

Note that some OFDM blocks might not experience the radar interference as in practice the radar duty cycle is low while the communications signal has 100% duty cycle, i.e., $\tau_R \le T_C \le T_R$. Let $\mathcal{I}$ denote the set of OFDM block indices during which radar pulses take place, i.e., $\mathcal{I} = \left\{ \left\lfloor \frac{\mathrm{T_d} + nT_R}{T_C} \right\rfloor \middle| n \in \left[0 : \left\lfloor \frac{LT_C - \mathrm{T_d}}{T_R} \right\rfloor\right] \right\}$. Also define $\varepsilon_m := 1_{\{m\in\mathcal{I}\}}$ is the binary indicator of the event $m \in \mathcal{I}$.

For a rectangular radar waveform, the sampled radar signal in (19) is given by

$$v_{R,m}[n] = \begin{cases} \varepsilon_m A_R & c_m \le n < d_m \\ 0 & \text{otherwise,} \end{cases} \quad n \in [0 : N-1], \tag{21}$$

where A_R is its radar pulse amplitude, and c_m and d_m denote the start and end of the non-zero content of $v_{R,m}[n]$ and are given by

$$c_m := [\mathrm{N_d} - N_{CP}]^+ \cdot 1_{\{\varepsilon_m = 1\}} + 0 \cdot 1_{\{\varepsilon_m = 0\}}, \tag{22}$$

$$d_m := [n_R - N_{CP}]^+ \cdot 1_{\{\varepsilon_m = 1\}} + 1 \cdot 1_{\{\varepsilon_m = 0\}}, \tag{23}$$

where $n_R := \lfloor \frac{\tau_R + \mathrm{T_d}}{T_S} \rfloor$ indicates the end of the radar pulse at the OFDM receiver and $[x]^+ := \max(0, x)$. By further assuming that $\Delta_f N T_S$ is an integer, we can write (19) as (see [19] for detailed derivation)

$$\begin{aligned} I_{k,m} &:= A_{k,m} e^{j\Theta_{k,m}}, \quad k \in [0 : N-1],\ m \in [0 : L-1] \\ &\approx \begin{cases} \dfrac{\varepsilon_m A_R}{\sqrt{N}} (d_m - c_m)\, e^{j\psi_m} \\ \qquad k_N = 0 \\ \dfrac{\varepsilon_m A_R}{\sqrt{N}} \dfrac{|\sin(\pi k_N (d_m - c_m)/N)|}{\sin(\pi k_N / N)} e^{j\psi'_{k,m}} \\ \qquad k_N \in [1 : N-1] \end{cases} \end{aligned} \tag{24}$$

$$k_N := (k - \Delta_f N T_S)_N, \tag{25}$$

$$\psi'_{k,m} := \psi_m + \pi\beta_{k,m} - \pi\frac{k_N}{N}(d_m + c_m - 1), \tag{26}$$

ψ_m in (20),

$$\beta_{k,m} := \begin{cases} 0, & 0 \le \left(\dfrac{k_N(d_m - c_m)}{N}\right)_2 \le 1 \\ 1, & \text{else,} \end{cases} \tag{27}$$

and where $(a)_N$ denotes a modulo N. Notice that the amplitude and phase of the radar interference at the k^{th} subcarrier and m^{th} OFDM block, denoted as $A_{k,m}$ and $\Theta_{k,m}$ in (24), respectively, are functions of $\mathrm{N_d}$ (through c_m). Thus, the radar interference matrix $\mathbf{I}$ from the channel model in (18) can be expressed as a deterministic function of the random variable $\mathrm{N_d}$. Note also that the simplified expression in (24) is a good approximation of the actual interference in (19) for any $\Delta_f N T_S \in \mathbb{R}_+$ (i.e., when removing the assumption that $\Delta_f N T_S$ is an integer) [19].

The simplified expression in (24) asserts that for those OFDM symbols and subcarriers that experience the radar interference, the joint distribution of $(A_{k,m}, \Theta_{k,m})$ is dominated by a single amplitude for which the phase is

essentially uniform. This general conclusion from [19] is not restricted to rectangular radar pulses. Although here we have restricted attention to a rectangular radar pulse for analytical simplicity, other waveforms lead to qualitatively similar joint (amplitude and phase) distributions seen at the OFDM receiver, and are expected to lead to similar overall conclusions since our model requires only statistical knowledge of the phase. With this in mind, the following radar parameters are assumed to be known (or can be reliably estimated) at the OFDM receiver in our model: the radar pulse shape including the radar pulse width (τ_R) and the radar carrier frequency (f_R) are generally either public record or can be obtained from the corresponding entity (e.g., a weather radar station), and the dominant radar signal's amplitude can be estimated as explained in Section II-A.

We conclude this section with a couple of remarks.

The radar pulse can interfere with two OFDM blocks rather than only one block as assumed in the above derivation; in this case, the radar pulse will arrive towards the end of the m^{th} block and extend to the start of the $(m+1)^{\text{th}}$ block. Following [20] and references therein for ATC radars, we assume that the radar pulse width is smaller than the cyclic prefix interval, i.e., $\tau_R < T_{CP}$. Thus, the first part of the radar pulse affects the data part of the m^{th} block, which increases the chance that the receiver makes an error; its second part, however, corrupts only the cyclic prefix part of the $(m+1)^{\text{th}}$ block, which will not contribute to a higher error rate at the $(m+1)^{\text{th}}$ block as its data is not damaged. As a result, the time lag between the communications and radar signals at the receiver falls within the range of the start of the radar-interfered OFDM block and the end of that block. Hence, this time delay $\mathrm{N_d}$ is assumed uniform on $[0, T_C - \tau_R)$ or, equivalently, the sampled time delay $\mathrm{N_d} \sim \mathcal{U}\{[0 : N_C - n_w]\}$, where $n_w = \lfloor \frac{\tau_R}{T_S} \rfloor$ is the sampled radar pulse width.

Finally, for the case of $N = L = 1$ with the assumption that the radar PRI equals the OFDM symbol span, i.e., $T_R = T_C$, the amplitude of the radar signal in (24) is approximately deterministic and its phase $\Theta_{k,m} = f(\mathrm{N_d})$ is in fact $\Theta \sim \mathcal{U}[0,2\pi]$, as discussed in Section II.

B. Detection Schemes

Based on the channel model of an OFDM receiver suffering from radar interference in (18), we can finally derive its corresponding detection schemes. The conditional distribution of the channel output $\mathbf{Y} = \mathbf{y} \in \mathbb{C}^{NL\times 1}$ in (18) given the communications input $\mathbf{X} = \mathbf{x} \in \mathbb{C}^{NL\times 1}$ and the random time delay $\mathrm{N_d} = n_d \in \mathbb{N}$ is given by

$$f_{\mathbf{Y}|\mathbf{X},\mathrm{N_d}}(\mathbf{y}|\mathbf{x}, n_d) = \frac{e^{-\|\mathbf{y}-\sqrt{\mathbf{S}}\mathbf{x}-\mathbf{i}(n_d)\|^2}}{\pi^{NL}}, \tag{28}$$

where the radar interference matrix $\mathbf{i}(n_d) \in \mathbb{C}^{NL\times 1}$ is a function of the random variable $\mathrm{N_d}$ with entries from (24) as mentioned previously.

This unknown time delay $\mathrm{N_d}$ causes the received signal to be correlated in both time and frequency according to $f_{\mathbf{Y}|\mathbf{X}}(\mathbf{y}|\mathbf{x}) = \mathbb{E}[f_{\mathbf{Y}|\mathbf{X},\mathrm{N_d}}(\mathbf{y}|\mathbf{x}, \mathrm{N_d})]$ with $\mathrm{N_d}$ uniformly distributed over $[0 : N_C - n_w]$. The optimal ML detector decodes N subcarriers and L blocks altogether. The suboptimal ML detectors are categorized into three cases, based on the correlation of the received signal: when it considers the correlation in time only (referred to as the suboptimal time-correlated decoder); when it considers the correlation in frequency only (referred to as the suboptimal frequency-correlated decoder); and when it considers the received signal as uncorrelated (referred to as the suboptimal symbol-by-symbol detector). Next, we derive the decoding schemes for these decoders that minimize the probability of error.

1) Optimal ML Decoder: Based on the channel conditional distribution in (28), the OPTIMAL receiver chooses an estimate of the transmitted symbol $\mathbf{X} = \mathbf{x}_\ell \in \mathbb{C}^{NL\times 1}$ for the received signal $\mathbf{Y} = \mathbf{y} \in \mathbb{C}^{NL\times 1}$

$$\hat{\ell}^{(\text{OPT})}(\mathbf{y}) = \underset{\substack{\mathbf{x}_\ell \in \{\mathbf{x}_1, \mathbf{x}_2, \ldots, \mathbf{x}_{M^{NL}}\} \\ \mathbf{x}_\ell = [x_1 \;\; x_2 \ldots x_{NL}]^T}}{\arg\max} \frac{1}{\pi^{NL}(N_C - n_w + 1)} \sum_{n_d=0}^{N_C - n_w} e^{-\sum_{m=0}^{L-1}\sum_{k=0}^{N-1} |[\mathbf{y}]_{k,m} - \sqrt{S_{k,m}}[\mathbf{x}_\ell]_{k,m} - i_{k,m}(n_d)|^2}, \tag{29}$$

where $[\mathbf{a}]_{k,m}$ denotes the k^{th} subcarrier and m^{th} block of $\mathbf{a}$.

2) Suboptimal Time-Correlated Decoder: The suboptimal time-correlated decoder ignores the correlation in frequency of the received signal and thus considers only the time correlation. We shall refer to this detector as the "SUBTIME" decoder. The SUBTIME receiver chooses an estimate of the transmitted symbol $\mathbf{X}' = \mathbf{x}'_\ell \in \mathbb{C}^{L\times 1}$ for the received signal $\mathbf{Y}' = \mathbf{y}' \in \mathbb{C}^{L\times 1}$ for all the blocks at the k^{th} subcarrier

$$\hat{\ell}_k^{(\text{SUBTIME})}(\mathbf{y}') = \underset{\substack{\mathbf{x}'_\ell \in \{\mathbf{x}'_1, \mathbf{x}'_2, \ldots, \mathbf{x}'_{M^L}\} \\ \mathbf{x}'_\ell = [x_1 \;\; x_2 \ldots x_L]^T}}{\arg\max} \frac{1}{\pi^{L}(N_C - n_w + 1)} \sum_{n_d=0}^{N_C - n_w} e^{-\sum_{m=0}^{L-1} |[\mathbf{y}']_{k,m} - \sqrt{S_{k,m}}[\mathbf{x}'_\ell]_{k,m} - i_{k,m}(n_d)|^2}. \tag{30}$$

The decoded block of size L at each k^{th} subcarrier in (30) are then put into a block of size NL, denoted as $\hat{\ell}^{(\text{SUBTIME})}(\mathbf{y}) \in \mathbb{C}^{NL\times 1}$, for the error rate analysis in Section III-C, and is given by

$$\hat{\ell}^{(\text{SUBTIME})}(\mathbf{y}) = \Big[\hat{\ell}_{k=0}^{(\text{SUBTIME})}(\mathbf{y}'|_{m=0}) \ldots \hat{\ell}_{k=N-1}^{(\text{SUBTIME})}(\mathbf{y}'|_{m=0}) \ldots \hat{\ell}_{k=0}^{(\text{SUBTIME})}(\mathbf{y}'|_{m=L-1}) \ldots \hat{\ell}_{k=N-1}^{(\text{SUBTIME})}(\mathbf{y}'|_{m=L-1})\Big]^T. \tag{31}$$

3) Suboptimal Frequency-Correlated Decoder: The suboptimal frequency-correlated decoder ignores the correlation in time of the received signal and thus considers only the frequency correlation. We shall refer to this detector as the "SUBFREQ" decoder. The SUBFREQ receiver chooses an estimate of the transmitted symbol $\mathbf{X}'' = \mathbf{x}''_\ell \in \mathbb{C}^{N\times 1}$ for the received signal $\mathbf{Y}'' = \mathbf{y}'' \in \mathbb{C}^{N\times 1}$ for all the subcarriers

at the m^{th} OFDM block

$$\hat{\ell}_m^{(\text{SUBFREQ})}(\mathbf{y}'') = \underset{\substack{\mathbf{x}''_\ell \in \{\mathbf{x}''_1, \mathbf{x}''_2, \ldots, \mathbf{x}''_{M^N}\} \\ \mathbf{x}''_\ell = [x_1 x_2 \ldots x_N]^T}}{\arg\max} \frac{1}{\pi^N (N_C - n_w + 1)} \sum_{n_d=0}^{N_C - n_w} e^{-\sum_{k=0}^{N-1} |[\mathbf{y}'']_{k,m} - \sqrt{S_{k,m}} [\mathbf{x}''_\ell]_{k,m} - i_{k,m}(n_d)|^2}. \quad (32)$$

The decoded block of size N at each m^{th} block in (32) are then put into a block of size NL, denoted as $\hat{\ell}^{(\text{SUBFREQ})}(\mathbf{y}) \in \mathbb{C}^{NL \times 1}$, for the error rate analysis in Section III-C, and is given by

$$\hat{\ell}^{(\text{SUBFREQ})}(\mathbf{y}) = \left[\hat{\ell}_{m=0}^{(\text{SUBFREQ})}(\mathbf{y}''); \ldots \hat{\ell}_{m=L-1}^{(\text{SUBFREQ})}(\mathbf{y}'') \right]. \quad (33)$$

4) Suboptimal Uncorrelated Decoder: The suboptimal uncorrelated decoder ignores the correlation in both frequency and time of the received signal and is basically a symbol-by-symbol detecter. We shall refer to this detector as the "SUBNONE" decoder. The SUBNONE receiver chooses an estimate of the transmitted symbol $X = x_\ell \in \mathbb{C}$ for the received signal $Y = y \in \mathbb{C}$ at the k^{th} subcarrier and m^{th} block

$$\hat{\ell}_{k,m}^{(\text{SUBNONE})}(y) = \underset{x_\ell \in \{x_1, x_2, \ldots, x_M\}}{\arg\max} \frac{1}{\pi (N_C - n_w + 1)} \sum_{n_d=0}^{N_C - n_w} e^{-|y_{k,m} - \sqrt{S_{k,m}} x_\ell - i_{k,m}(n_d)|^2}. \quad (34)$$

The decoded symbol at each m^{th} block and k^{th} subcarrier in (34) are then put into a block of size NL, denoted as $\hat{\ell}^{(\text{SUBNONE})}(\mathbf{y}) \in \mathbb{C}^{NL \times 1}$, for the error rate analysis in Section III-C, and is given by

$$\hat{\ell}^{(\text{SUBNONE})}(\mathbf{y}) = [\hat{\ell}_{0,0}^{(\text{SUBNONE})}(y) \ldots \hat{\ell}_{N-1,0}^{(\text{SUBNONE})}(y) \ldots \hat{\ell}_{0,L-1}^{(\text{SUBNONE})}(y) \ldots \hat{\ell}_{N-1,L-1}^{(\text{SUBNONE})}(y)]^T. \quad (35)$$

Since the optimal receiver decodes the whole block (of L symbols and N subcarriers) of the received signal, its computation time increases with the constellation size and numbers of subcarriers and symbols. The suboptimal receivers reduce the decoding time by disregarding some or all of the correlations in the received signal. Hence, the computational complexity (in terms of decoding time) for each decoder is:

- $O\left(M^{NL} \times NL \times (N_C - n_w)\right)$ for OPTIMAL decoder,
- $O\left(M^{L} \times NL \times (N_C - n_w)\right)$ for SUBTIME decoder,
- $O\left(M^{N} \times NL \times (N_C - n_w)\right)$ for SUBFREQ decoder, and
- $O\left(1 \times NL \times (N_C - n_w)\right)$ for SUBNONE decoder.

C. Error Rate Analysis and Results

We now study the performance of the receivers in terms of error rate. Here we look at two types of error rates: BLock Error Rate (BLER) and Symbol Error Rate (SER). We consider N_B blocks, where each block is of size NL constellation symbols (for all the L OFDM blocks and N subcarriers). The BLER looks counts all $\hat{\ell}(\mathbf{y})$ for each block and calculates how many blocks contain one or more symbol errors, while the SER looks at how many incorrect symbols occur on average in each $\hat{\ell}(\mathbf{y})$ block. Since the probability of the error event $f_{\mathbf{Y}|\mathbf{X}}(\mathbf{y}|\mathbf{x}_\ell) < \max_{k:k \neq \ell} f_{\mathbf{Y}|\mathbf{X}}(\mathbf{y}|\mathbf{x}_k)$, conditioned on $\mathbf{x}_\ell$ sent, does not seem to have a closed form expression, we proceed to use Monte Carlo simulation to approximate them. In particular, we evaluate the BLER and the SER as

$$\mathsf{BLER} \approx \frac{1}{N_B} \sum_{b=1}^{N_B} \varepsilon_b, \quad (36)$$

where ε_b is the indicator function for the b^{th} block that at least one symbol is in error, and

$$\mathsf{SER} \approx \frac{1}{NL \times N_B} \sum_{b=1}^{N_B} \sum_{s=1}^{NL} \varepsilon_{b,s}, \quad (37)$$

where $\varepsilon_{b,s}$ is the indicator function for an error in the s^{th} symbol of the b^{th} block.

Next we evaluate the error rate performance of the various decoders. The OFDM system operates at a carrier frequency of $f_C = 2.84952$ GHz (such that $\Delta_f N T_S$ is an integer) with a total bandwidth of $B_C = 960$ kHz. The cyclic prefix has a length of $N_{CP} = 16$. The selection of the available bandwidth is consistent with an LTE communications system. The pulsed radar system transmits a rectangular pulse of amplitude $A_R = 2.5$ every $T_R = 83.33\ \mu s$ at a carrier frequency of $f_R = 2.85$ GHz. Based on the decoders in (29), (31), (33), and (35) with the rectangular radar interference in (24), we conduct various evaluations with different values for the number of subcarriers N, number of OFDM blocks L, and sampled radar pulse width n_w. The modulation schemes considered in this example are Binary Phase-Shift Keying (BPSK), PAM, and QAM, which are the commonly-used signal constellations.

Table VI shows the BLER and SER performances of all the decoders with $\mathsf{S} = 10$ dB at each subcarrier. As expected, numerical results indicate that the OPTIMAL decoder always outperforms the suboptimal decoders in terms of error rates, both block and symbol, and that the SUBNONE decoder (symbol-by-symbol detector) generally performs the worst as it ignores all the correlations. The SUBTIME decoder is optimal when there is only 1 channel in the system (i.e., $N = 1$) as there is no correlation in frequency. Similarly, the SUBFREQ decoder becomes optimal when there is only 1 OFDM block (i.e., $L = 1$) as there is no correlation in time. Generally, the SUBFREQ decoder performs competitively with (but usually slightly better than) the SUBNONE decoder; however, it does not perform as well as the SUBTIME decoder. This indicates that accounting for time correlation (i.e., decoding several OFDM blocks at once at the expense of increased complexity) is critical for good performance. There is a trade off between the computation time and error rates when using suboptimal decoders. Depending on an application, if the time complexity is a major constraint (especially for large values of M, N, and L) then the SUBTIME decoder is an excellent compromise. Notice that both the BLERs and SERs increase with the constellation size for the same system configurations as seen in the case where M increases from 2 to 4 (i.e., the third to fifth rows in Table VI), in which BPSK yields

TABLE VI

ERROR RATE (IN LOG-SCALE) COMPARISON FOR VARIOUS DECODERS, FOR DIFFERENT NUMBERS OF SUBCARRIERS N, OF OFDM BLOCKS L, AND SAMPLED RADAR PULSE WIDTH n_w

Parameters \ Decoders	OPTIMAL	SUBTIME	SUBFREQ	SUBNONE
$N=2,\ L=1$ $n_w=2$, BPSK	$\log(\mathsf{BLER})=-2.343$ $\log(\mathsf{SER})=-2.644$	$\log(\mathsf{BLER})=-2.338$ $\log(\mathsf{SER})=-2.639$	$\log(\mathsf{BLER})=-2.343$ $\log(\mathsf{SER})=-2.644$	$\log(\mathsf{BLER})=-2.338$ $\log(\mathsf{SER})=-2.639$
$N=2,\ L=2$ $n_w=1$, BPSK	$\log(\mathsf{BLER})=-4.444$ $\log(\mathsf{SER})=-5.046$	$\log(\mathsf{BLER})=-3.688$ $\log(\mathsf{SER})=-4.288$	$\log(\mathsf{BLER})=-3.638$ $\log(\mathsf{SER})=-4.237$	$\log(\mathsf{BLER})=-3.269$ $\log(\mathsf{SER})=-3.871$
$N=2,\ L=2$ $n_w=2$, BPSK	$\log(\mathsf{BLER})=-3.221$ $\log(\mathsf{SER})=-3.656$	$\log(\mathsf{BLER})=-3.217$ $\log(\mathsf{SER})=-3.652$	$\log(\mathsf{BLER})=-2.035$ $\log(\mathsf{SER})=-2.630$	$\log(\mathsf{BLER})=-2.032$ $\log(\mathsf{SER})=-2.627$
$N=2,\ L=2$ $n_w=2$, 4-QAM	$\log(\mathsf{BLER})=-1.673$ $\log(\mathsf{SER})=-2.075$	$\log(\mathsf{BLER})=-1.560$ $\log(\mathsf{SER})=-1.996$	$\log(\mathsf{BLER})=-1.243$ $\log(\mathsf{SER})=-1.755$	$\log(\mathsf{BLER})=-1.177$ $\log(\mathsf{SER})=-1.697$
$N=2,\ L=2$ $n_w=2$, 4-PAM	$\log(\mathsf{BLER})=-0.800$ $\log(\mathsf{SER})=-1.302$	$\log(\mathsf{BLER})=-0.800$ $\log(\mathsf{SER})=-1.302$	$\log(\mathsf{BLER})=-0.751$ $\log(\mathsf{SER})=-1.258$	$\log(\mathsf{BLER})=-0.751$ $\log(\mathsf{SER})=-1.258$
$N=2,\ L=4$ $n_w=2$, BPSK	$\log(\mathsf{BLER})=-4.523$ $\log(\mathsf{SER})=-5.347$	$\log(\mathsf{BLER})=-4.523$ $\log(\mathsf{SER})=-5.347$	$\log(\mathsf{BLER})=-1.747$ $\log(\mathsf{SER})=-2.630$	$\log(\mathsf{BLER})=-1.744$ $\log(\mathsf{SER})=-2.627$
$N=4,\ L=2$ $n_w=2$, BPSK	$\log(\mathsf{BLER})=-2.608$ $\log(\mathsf{SER})=-3.214$	$\log(\mathsf{BLER})=-2.531$ $\log(\mathsf{SER})=-3.175$	$\log(\mathsf{BLER})=-1.751$ $\log(\mathsf{SER})=-2.634$	$\log(\mathsf{BLER})=-1.746$ $\log(\mathsf{SER})=-2.629$
$N=4,\ L=2$ $n_w=4$, BPSK	$\log(\mathsf{BLER})=-2.122$ $\log(\mathsf{SER})=-2.726$	$\log(\mathsf{BLER})=-1.947$ $\log(\mathsf{SER})=-2.557$	$\log(\mathsf{BLER})=-1.375$ $\log(\mathsf{SER})=-2.210$	$\log(\mathsf{BLER})=-1.340$ $\log(\mathsf{SER})=-2.122$
$N=4,\ L=4$ $n_w=2$, BPSK	$\log(\mathsf{BLER})=-3.604$ $\log(\mathsf{SER})=-4.285$	$\log(\mathsf{BLER})=-3.457$ $\log(\mathsf{SER})=-4.234$	$\log(\mathsf{BLER})=-1.492$ $\log(\mathsf{SER})=-2.640$	$\log(\mathsf{BLER})=-1.488$ $\log(\mathsf{SER})=-2.635$

the lowest error rates while 4-PAM gives the highest error rates. Notice also that an increase in the radar pulse width degrades the performance of the system as seen in the case where n_w increases from 2 to 4 (i.e., the seventh and eighth rows in Table VI).

We finally conclude that among all the suboptimal decoders, the SUBTIME receiver consistently yields the lowest error rates except for the case when $L=1$ in which the SUBFREQ receiver outperforms the SUBTIME receiver (i.e., the first row in Table VI).

IV. CONCLUSIONS

In this paper, we investigated a single-carrier system subject to radar interference. The analysis of the symbol error rate showed that the communications receiver should treat the radar interference of weak power as Gaussian noise, while it should subtract the radar interference of very strong power off the received signal. The latter unfortunately results in a loss of one of the two real-valued dimensions in the complex-valued received signal, which has been shown to be unavoidable in [25]. We then considered the designs of a two-dimensional signal constellation able to better (than classical constellations) handle this particular radar interference from two perspectives: maximizing the transmission rate subject to average power and error rate constraints, and minimizing the error rate subject to a power constraint and a fixed rate condition. We observed that the optimally designed constellation tends to a concentric hexagon shape for low power radar interference and to an unequally-spaced PAM shape for high power radar interference. Although the detection scheme for the radar interference of intermediate power cannot be expressed in a closed-form, the result showed that the designed constellation is shaped as a transition from a hexagonal-like shape at weak radar interference to a PAM-like shape at very strong radar interference. These findings may be of guidance in effectively co-designing, or at least offer a baseline for comparison when radar and communications systems share the same spectrum.

We also discussed a more complicated but practically relevant model of a multi-carrier communications system. We modeled the additive pulsed radar interference after being processed by an OFDM receiver and analyzed several optimal (in terms of minimizing the probability of error) and suboptimal detection schemes. The unknown time lag between the radar interference and communications signal, modeled as a random variable, causes the received communications signal to be correlated in both time and frequency. We categorized the suboptimal decoders, based on the correlation, into three types: the suboptimal time-correlated decoder considers the correlation in time only; the suboptimal frequency-correlated decoder considers the correlation in frequency only; while the suboptimal uncorrelated decoder, also known as the symbol-by-symbol detector, ignores the correlation in both time and frequency. We evaluated the error rate performances of the receivers with an interfering rectangular radar signal via simulations and the result showed that the suboptimal time-correlated receiver performs the best while the suboptimal symbol-by-symbol receiver performs the worst.

APPENDIX A
EQUIVALENT REAL-VALUED PHASE-FADING GAUSSIAN CHANNEL FOR VERY STRONG RADAR INTERFERENCE

The IC decoder in (6) is an approximation of the optimal ML decoder in (4) when $\mathsf{I} \gg \mathsf{S} \gg 1$ and can be rewritten as

$$\begin{aligned}\hat{\ell}^{(\mathrm{IC})}(y) &= \underset{\ell\in[1:M]}{\arg\min}\left(|y-\sqrt{\mathsf{S}}x_\ell|-\sqrt{\mathsf{I}}\right)^2 \\ &= \underset{\ell\in[1:M]}{\arg\min}\left(\frac{|y-\sqrt{\mathsf{S}}x_\ell|^2-\mathsf{I}}{|y-\sqrt{\mathsf{S}}x_\ell|+\sqrt{\mathsf{I}}}\right)^2. \end{aligned} \tag{38}$$

$$
\begin{aligned}
|y-\sqrt{\mathsf{S}}x_\ell|^2-\mathsf{I} &= |(\sqrt{\mathsf{S}}x-\sqrt{\mathsf{S}}x_\ell+z)+\sqrt{\mathsf{I}}e^{j\Theta}|^2-\mathsf{I} \\
&= 2\sqrt{\mathsf{I}}\left[\frac{|\sqrt{\mathsf{S}}x-\sqrt{\mathsf{S}}x_\ell+z|^2}{2\sqrt{\mathsf{I}}}+\Re\{e^{-j\Theta}(\sqrt{\mathsf{S}}x-\sqrt{\mathsf{S}}x_\ell+z)\}\right] \\
&\overset{\mathsf{I}\gg\mathsf{S}}{=} 2\sqrt{\mathsf{I}}\left[O\left(\sqrt{\mathsf{S}/\mathsf{I}}\right)+\left(y_{\text{eq}}-\Re\{e^{-j\Theta}\sqrt{\mathsf{S}}x_\ell\}\right)\right], \qquad (39)
\end{aligned}
$$

$$
\begin{aligned}
|y-\sqrt{\mathsf{S}}x_\ell|+\sqrt{\mathsf{I}} &= \sqrt{\mathsf{I}}\left[1+\sqrt{\frac{|\sqrt{\mathsf{S}}x-\sqrt{\mathsf{S}}x_\ell+z|^2}{\mathsf{I}}+\frac{2\Re\{e^{-j\Theta}(\sqrt{\mathsf{S}}x-\sqrt{\mathsf{S}}x_\ell+z)\}}{\sqrt{\mathsf{I}}}+1}\right] \\
&\overset{\mathsf{I}\gg\mathsf{S}}{=} 2\sqrt{\mathsf{I}}\left[1+O\left(\sqrt{\mathsf{S}/\mathsf{I}}\right)\right], \qquad (40)
\end{aligned}
$$

The numerator and the denominator in (38), by letting $y=\sqrt{\mathsf{S}}x+\sqrt{\mathsf{I}}e^{j\Theta}+z$, can be approximated as where in (39), shown at the top of this page, we defined

$$y_{\text{eq}} := \Re\{e^{-j\Theta}(\sqrt{\mathsf{S}}x+z)\}=\Re\{e^{-j\Theta}(y-\sqrt{\mathsf{I}}e^{j\Theta})\}, \quad (41)$$

and $O(\cdot)$ denotes the big "O" notation, i.e., $f(x)=O(g(x))$ if and only if there exists a positive real number κ and an x_0 such that $|f(x)|\le\kappa|g(x)|$ for all $x\ge x_0$. Therefore, by combining (39) and (40), as shown at the top this page, we see that, in the regime $\mathsf{I}\gg\mathsf{S}\gg 1$, the IC decoder in (38) can be approximated as

$$\hat{\ell}^{(\text{IC})}(y)\overset{\mathsf{I}\gg\mathsf{S}}{\approx}\arg\min_{\ell\in[1:M]}\left(y_{\text{eq}}-\Re\{e^{-j\Theta}\sqrt{\mathsf{S}}x_\ell\}\right)^2=:\hat{\ell}^{(\text{ML})}(y_{\text{eq}}). \quad (42)$$

The right hand side of (42) is the optimal ML decoder of a real-valued phase-fading Gaussian channel with fading Θ known at the receiver; that is, for a channel with input $X\in\mathbb{C}$ and output $(Y_{\text{eq}},\Theta)\in\mathbb{R}^2$ where

$$Y_{\text{eq}} := \sqrt{\mathsf{S}}\Re\{e^{-j\Theta}X\}+Z_{\text{eq}}\in\mathbb{R}, Z_{\text{eq}}\sim\mathcal{N}_R(0,\frac{1}{2}). \quad (43)$$

Another *interpretation* of (42) based on the right hand side of (41) is that the decoder receives y then estimates and "compensates" for the radar phase Θ but in doing so one of the two real-valued dimensions of the received signal is lost.

Appendix B
Proof of the SER for an M-PAM for Very Strong Radar Interference

The probability of error at high INR for the IC decoder in (12) when an M-PAM with equally-likely unit-energy input symbols is used, can be found as follows. We note that

$$\left|r_k(\Theta)-r_\ell(\Theta)\right|=\left|x_k\cos(\Theta)-x_\ell\cos(\Theta)\right|=d_{k,\ell}|\cos(\Theta)|,$$

and therefore we do not need to distinguish various cases depending on the $\text{sign}\,(r_k(\Theta)-r_\ell(\Theta))$. With this, we have the following expressions for (14) and (15)

$$\Delta^+_{k,\ell}(\Theta)=\Delta^-_{k,\ell}(\Theta)=\sqrt{\frac{\mathsf{S}}{2}d^2_{\min}\cos^2(\Theta)}$$

and thus,

$$Q\left(\Delta^+_{k,\ell}(\Theta)\right)=Q\left(\Delta^-_{k,\ell}(\Theta)\right)=Q\left(\sqrt{\frac{6\mathsf{S}}{M^2-1}\cos^2(\Theta)}\right).$$

Finally, for an M-PAM we get the exact probability of error

$$
\begin{aligned}
P^{(\text{ML})}_{\text{e,PAM}} &\le P^{(\text{IC})}_{\text{e,PAM}}\overset{\mathsf{I}\gg\mathsf{S}\gg 1}{\approx}\frac{1}{M}\sum_{\ell=1}^{M}\mathbb{E}_\Theta\left[Q\left(\Delta^+_{k,\ell}(\Theta)\right)+Q\left(\Delta^-_{k,\ell}(\Theta)\right)\right] \\
&= \frac{2}{M}\mathbb{E}_\Theta\left[1\cdot Q\left(\sqrt{\frac{6\mathsf{S}}{M^2-1}\cos^2(\Theta)}\right)\right] \\
&\quad+\frac{M-2}{M}\mathbb{E}_\Theta\left[2\cdot Q\left(\sqrt{\frac{6\mathsf{S}}{M^2-1}\cos^2(\Theta)}\right)\right] \\
&= 2\left(1-\frac{1}{M}\right)\mathbb{E}_\Theta\left[Q\left(\sqrt{\frac{6\mathsf{S}}{M^2-1}\cos^2(\Theta)}\right)\right].
\end{aligned}
$$

Appendix C
SER Performance for a PAM Constellation

Here we show the error rate as a function of SNR and INR; the regime of interest is when both SNR and INR are above 0 dB. Fig. 3(a) [26, Fig. 3] shows the Bit Error Rate (BER) versus S and I in dB for the optimal decoder for a 2-PAM constellation; similar plots can be obtained for other constellations. It can be seen that at fixed SNR, the BER increases with INR up to some point around INR $\cong$ SNR, then the BER starts to decrease and flattens out to an asymptote, which can be characterized in closed form as $2(1-\frac{1}{M})\mathbb{E}_\Theta\left[Q\left(\sqrt{\frac{6\mathsf{S}}{M^2-1}\cos^2(\Theta)}\right)\right]$ for an M-PAM; this 'slice' of the error rate curve for a fixed SNR is what we chose to show in Figs. 1 and 2. For a fixed INR >0, the BER first decays polynomially with SNR for SNR $<$ INR (i.e., high INR regime; IC decoder approximately optimal) and then it decays exponentially to zero for SNR $>$ INR (i.e., low INR regime; TIN decoder approximately optimal). The ridge around INR $\cong$ SNR, where the error rate attains its highest value, is an undesirable operating point; we do not have an intuitive explanation as to why the 'peak' happens at around INR $\cong$ SNR except that the radar interference is neither low enough to be 'neglected' or treated as a Gaussian noise (i.e., low INR regime; TIN decoder approximately optimal), nor 'strong' enough to be accounted for (i.e., high INR regime; IC decoder approximately optimal).

The SER versus S in dB curves for a PAM constellation of size $M=$ 2,4, and 8 is shown in Fig. 3(b); two sets of

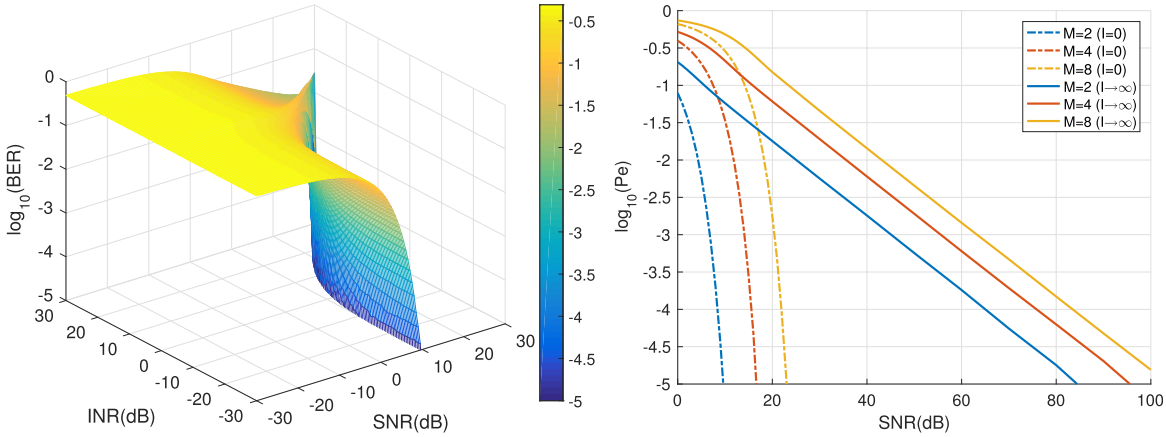

(a) BER (in log scale) vs. S and I in dB.

(b) SER comparison vs. S_{dB} for various M values.

Fig. 3. Error rate comparisons

curves are depicted: (1) $\mathsf{I} = 0$ (the AWGN-only channel) and (2) $\mathsf{I} \to \infty$ (the real-valued phase-fading channel). The curves corresponding to a 2-PAM are slices of Fig. 3(a); we notice that other M-PAM's behave qualitatively like the 2-PAM constellation. Note also that imposing $\log_{10}(\text{SER}) \leq -3$ requires $\mathsf{S}_{\text{dB}} \geq 45$ for $M = 2$, $\mathsf{S}_{\text{dB}} \geq 55$ for $M = 4$, and $\mathsf{S}_{\text{dB}} \geq 63$ for $M = 8$. Therefore, the proposed constellations yield higher error rates than the tolerable SER in practice since the SNR range used in our examples in Section II-E are low.

REFERENCES

[1] (May 2016). *Enhancing Access to the Radio Spectrum (EARS)*. [Online]. Available: http://www.nsf.gov/funding/pgm_summ.jsp?pims_id=503480

[2] (2012). *Shared Spectrum Access for Radar and Communications (SSPARC)*. [Online]. Available: http://www.darpa.mil/program/shared-spectrum-access-for-radar-and-communications

[3] H. Shajaiah, A. Khawar, A. Abdel-Hadi, and T. C. Clancy, "Resource allocation with carrier aggregation in LTE advanced cellular system sharing spectrum with S-band radar," in *Proc. IEEE Int. Symp. Dyn. Spectr. Access Netw. (DYSPAN)*, Apr. 2014, pp. 34–37.

[4] R. A. Romero and K. D. Shepherd, "Friendly spectrally shaped radar waveform with legacy communication systems for shared access and spectrum management," *IEEE Access*, vol. 3, pp. 1541–1554, Aug. 2015.

[5] M. Mehrnoush and S. Roy, "Interference mitigation in coexistence of WLAN network with radar," in *Proc. IEEE Radar Conf. (RadarConf)*, Seattle, WA, USA, May 2017, pp. 0257–0262.

[6] L. Zheng, M. Lops, X. Wang, and E. Grossi, "Joint design of overlaid communication systems and pulsed radars," *IEEE Trans. Signal Process.*, vol. 66, no. 1, pp. 139–154, Jan. 2017.

[7] B. Li, H. Kumar, and A. P. Petropulu, "A joint design approach for spectrum sharing between radar and communication systems," in *Proc. IEEE Int. Conf. Acoust., Speech Signal Process. (ICASSP)*, Shanghai, China, Mar. 2016, pp. 3306–3310.

[8] A. D. Harper, J. T. Reed, J. L. Odom, A. D. Lanterman, and X. Ma, "Performance of a linear-detector joint radar-communication system in doubly selective channels," *IEEE Trans. Aerosp. Electron. Syst.*, vol. 23, no. 2, pp. 703–715, Apr. 2017.

[9] Y. Zhang, Q. Li, L. Huang, C. Pan, and J. Song, "A modified waveform design for radar-communication integration based on LFM-CPM," in *Proc. IEEE 85th Veh. Technol. Conf. (VTC Spring)*, Sydney, NSW, Australia, Jun. 2017, pp. 1–5.

[10] M. A. Dida, H. Hao, X. Wang, and T. Ran, "Constant envelope chirped OFDM for power-efficient radar communication," in *Proc. IEEE Inf. Technol., Netw., Electron. Autom. Control Conf.*, Chongqing, China, Sep. 2016, pp. 298–301.

[11] C. Sahin, J. Jakabosky, P. M. McCormick, J. G. Metcalf, and S. D. Blunt, "A novel approach for embedding communication symbols into physical radar waveforms," in *Proc. IEEE Radar Conf. (RadarConf)*, Seattle, WA, USA, May 2017, pp. 1498–1503.

[12] C. Shi, F. Wang, M. Sellathurai, J. Zhou, and S. Salous, "Power minimization-based robust OFDM radar waveform design for radar and communication systems in coexistence," *IEEE Trans. Signal Process.*, vol. 66, no. 5, pp. 1316–1330, Nov. 2017.

[13] B. Li and A. Petropulu, "Joint transmit designs for co-existence of MIMO wireless communications and sparse sensing radars in clutter," *IEEE Trans. Aerosp. Electron. Syst.*, vol. 53, no. 6, pp. 2846–2864, Dec. 2017.

[14] H. Zheng, Y. Li, and Y. Zhu, "The communication solution for LTE system under radar interference circumstance," *Int. J. Antennas Propag.*, vol. 2015, 2015, Art. no. 849695, doi: 10.1155/2015/849695.

[15] H. Wang, J. T. Johnson, and C. J. Baker, "Spectrum sharing between communications and ATC radar systems," *IET Radar, Sonar Navigat.*, vol. 11, no. 6, pp. 994–1001, Jul. 2017.

[16] D. P. Zilz and M. R. Bell, "Statistical modeling of wireless communications interference and its effects on adaptive-threshold radar detection," *IEEE Trans. Aerosp. Electron. Syst.*, Nov. 2017.

[17] N. Nartasilpa, D. Tuninetti, N. Devroye, and D. Erricolo, "On the error rate of a communication system suffering from additive radar interference," in *Proc. IEEE Global Commun. Conf. (GlobeCom)*, Washington, DC, USA, Dec. 2016, pp. 1–6.

[18] N. Nartasilpa, D. Tuninetti, and N. Devroye, "Signal constellation design in the presence of radar interference and Gaussian noise," in *Proc. IEEE Military Commun. Conf. (MILCOM)*, Baltimore, MD, USA, Oct. 2017, pp. 719–724.

[19] A. Salim, D. Tuninetti, N. Devroye, and D. Erricolo, "Modeling the interference of pulsed radar signals in OFDM-based communications systems," in *Proc. IEEE Radar Conf. (RadarConf)*, Seattle, WA, USA, May 2017, pp. 0657–0662.

[20] S. Heuel, D. McCarthy, and Y. Shavit, "Test and measurement of coexistence between S-Band radar and mobile networks," in *Proc. 26th Int. Conf. Radioelektronika*, Apr. 2016, pp. 1–4.

[21] A. Goldsmith, *Wireless Communications*, 2nd ed. Cambridge, U.K.: Cambridge University Press, 2005.

[22] M. Abramovitz and I. A. Stegun, *Handbook of Mathematical Functions*. New York, NY, USA: Dover, 1970.

[23] J. G. Proakis, *Digital Communications*, 5th ed. New York, NY, USA: McGraw-Hill, 2007.

[24] Z. Ugray, L. Lasdon, J. Plummer, F. Glover, J. Kelly, and R. Mart, "Scatter search and local NLP solvers: A multistart framework for global optimization," *Inf. J. Comput.*, vol. 19, no. 3, pp. 328–340, 2007.

[25] S. Shahi, D. Tuninetti, and N. Devroye, "On the capacity of the AWGN channel with additive radar interference," in *Proc. 54th Annu. Allerton Conf. Commun., Control, Comput.*, Monticello, IL, USA, Sep. 2016, pp. 902–907.

[26] N. Nartasilpa, D. Tuninetti, N. Devroye, and D. Erricolo, "Let's share CommRad: Effect of radar interference on an uncoded data communication system," in *Proc. IEEE Radar Conf. (RadarConf)*, Philadelphia, PA, USA, May 2016, pp. 1–5.

Narueporn Nartasilpa received the B.Eng. degree in electrical engineering from Kasetsart University in 2008 and the M.S. degree in electrical engineering from Florida International University, Miami, FL, USA, in 2011. She is currently pursuing the Ph.D. degree from the University of Illinois at Chicago, Chicago, IL, USA. Her current research topic focuses on communications system performance in the presence of radar interference and the information theoretic joint-design of coexisting radar and communications systems. She has served as a Reviewer for the IEEE TRANSACTIONS ON COMMUNICATIONS and the IEEE TRANSACTIONS ON COGNITIVE COMMUNICATIONS AND NETWORKING.

Ahmad Salim received the B.Sc. degree in electrical engineering from the University of Jordan, Amman, Jordan, in 2006, the M.Sc. degree in telecommunication engineering from the King Fahd University of Petroleum and Minerals, Dhahran, Saudi Arabia, in 2010, and the Ph.D. degree in electrical engineering from Arizona State University, Tempe, AZ, USA, in 2015. He is currently a Post-Doctoral Research Associate with the Department of Electrical and Computer Engineering, University of Illinois at Chicago, Chicago, IL, USA. His research belongs to the areas of communications theory, information theory and signal processing, including wireless communications, underwater acoustic communications, cooperative communications, MIMO systems, diversity techniques, error control coding, and iterative receivers.

Dr. Salim achieved eighth place in Jordan's 2006 nationwide comprehensive examination in the electrical engineering discipline. He is an active participant of the Sensor, Signal and Information Processing Center, Arizona State University. He is a member of the Communication Theory Technical Committee. He served as a Reviewer for the IEEE TRANSACTIONS ON WIRELESS COMMUNICATIONS, the IEEE WIRELESS COMMUNICATIONS LETTERS, the IEEE TRANSACTIONS ON VEHICULAR TECHNOLOGY, *Physical Communication* (Elsevier), and among others.

Daniela Tuninetti received the Ph.D. degree in electrical engineering from ENST/Telecom ParisTech, Paris, France, in 2002 (with work done at the Eurecom Institute, Sophia Antipolis, France). She was a Post-Doctoral Research Associate with the School of Communication and Computer Science, Swiss Federal Institute of Technology in Lausanne, Lausanne, Switzerland, from 2002 to 2004. In 2005 she joined the Department of Electrical and Computer Engineering, University of Illinois at Chicago, Chicago, IL, USA, where she is currently a Professor. She was a recipient of a best paper award at the European Wireless Conference in 2002, an NSF CAREER award in 2007, and named UIC University Scholar in 2015.

Her research interests are in the ultimate performance limits of wireless interference networks (with special emphasis on cognition and user cooperation), coexistence between radar and communication systems, multi-relay networks, content-type coding, and caching systems. She was an Editor-in-Chief of the *IEEE Information Theory Society Newsletter* from 2006 to 2008, an Editor for the IEEE COMMUNICATION LETTERS from 2006 to 2009, and for the IEEE TRANSACTIONS ON WIRELESS COMMUNICATIONS from 2011 to 2014. She is currently an Associate Editor for the IEEE TRANSACTIONS ON INFORMATION THEORY.

Natasha Devroye received the B.Eng. degree (Hons.) in electrical engineering from McGill University in 2001 and the Ph.D. degree in engineering sciences from the School of Engineering and Applied Sciences, Harvard University, Cambridge, MA, USA, in 2007. From 2007 to 2008 she was a Lecturer with Harvard University. In 2009, she joined the Department of Electrical and Computer Engineering, University of Illinois at Chicago (UIC), Chicago, IL, USA, where she is currently an Associate Professor.

Her research focuses on multi-user information theory and applications to cognitive and software-defined radio, radar, relay, zero-error, and two-way communication networks. She was a recipient of an NSF CAREER award in 2011 and was named UIC's Researcher of the Year in the Rising Star category in 2012. She has been an Associate Editor for the IEEE TRANSACTIONS ON WIRELESS COMMUNICATIONS, the IEEE JOURNAL OF SELECTED AREAS IN COMMUNICATIONS, and is currently an Associate Editor for the IEEE TRANSACTIONS ON COGNITIVE COMMUNICATIONS AND NETWORKING and the IEEE TRANSACTIONS ON INFORMATION THEORY.